TUM–HEP–365/99
OUTP–99–69P
SISSA 151/99/EP

# Testing Matter Effects in Very Long Baseline Neutrino Oscillation Experiments*

M. Freund[a], M. Lindner[b], S. T. Petcov[c,d] and A. Romanino[e]

[a,b] *Theoretische Physik, Physik Department, Technische Universität München, James–Franck–Strasse, D–85748 Garching, Germany*

[c] *Scuola Internazionale Superiore di Studi Avanzati, and INFN - Sezione de Trieste, I-34014 Trieste, Italy*

[e] *Department of Physics, Theoretical Physics, University of Oxford, Oxford OX13NP, UK*



## Abstract

Assuming three-neutrino mixing, we study the capabilities of very long baseline neutrino oscillation experiments to verify and test the MSW effect and to measure the lepton mixing angle $\theta_{13}$. We suppose that intense neutrino and antineutrino beams will become available in so–called neutrino factories. We find that the most promising and statistically significant results can be obtained by studying $\nu_e \to \nu_\mu$ and $\bar{\nu}_e \to \bar{\nu}_\mu$ oscillations which lead to matter enhancements and suppressions of wrong sign muon rates. We show the $\theta_{13}$ ranges where matter effects could be observed as a function of the baseline. We discuss the scaling of rates, significances and sensitivities with the relevant mixing angles and experimental parameters. Our analysis includes fluxes, event rates and statistical aspects so that the conclusions should be useful for the planning of experimental setups. We discuss the subleading $\Delta m^2_{21}$ effects in the case of the LMA MSW solution of the solar problem, showing that they are small for $L \gtrsim 7000\,\text{km}$. For shorter baselines, $\Delta m^2_{21}$ effects can be relevant and their dependence on $L$ offers a further handle for the determination of the CP-violation phase $\delta$. Finally we comment on the possibility to measure the specific distortion of the energy spectrum due to the MSW effect.

*Work supported in part by "Sonderforschungsbereich 375 für Astro-Teilchenphysik" der Deutschen Forschungsgemeinschaft, by the TMR Network under the EEC Contract No. ERBFMRX–CT960090 and by the Italian MURST under the program "Fisica Teorica delle Interazioni Fondamentali".

[a]Email: Martin.Freund@physik.tu-muenchen.de
[b]Email: Manfred.Lindner@physik.tu–muenchen.de
[c]Email: petcov@he.sissa.it
[d]Also at: INRNE, Bulgarian Academy of Sciences, 1789 Sofia, Bulgaria.
[e]Email: romanino@thphys.ox.ac.uk

# 1 Introduction

The long term aim to build muon colliders offers the very attractive intermediate possibility for "neutrino factories" [1, 2, 3] with uniquely intense and precisely characterized neutrino and antineutrino beams. This requires only one muon beam at intermediate energies such that neutrino factories are rather realistic medium term projects which constitute also a useful step in accelerator technology towards a muon collider. The current knowledge of neutrino masses and mixing implies for typical setups very promising very long baseline neutrino experiments. We study in this paper in a three neutrino framework the potential to verify and test the MSW effect and to measure or limit $\theta_{13}$ in terrestrial very long baseline experiments with neutrino factories where the neutrino spectrum and fluxes are rather well known and under control [1]. Calculating the oscillation probabilities and event rates for different channels and comparing with those for oscillations in vacuum we find that the asymmetry between the $\nu_e \leftrightarrow \nu_\mu$ and $\bar{\nu}_e \leftrightarrow \bar{\nu}_\mu$ oscillations is a very promising tool to test and verify the MSW effect. The reason is, as we will see, that matter effects lead to measurably enhanced event rates in one of the two channels and to equally suppressed transitions in the other. The asymmetry between the event rates associated with these two channels would therefore be very sensitive to the MSW effect since the matter induced changes have opposite effect on the two rates thus amplifying the "signal", while at the same time common backgrounds would drop out. We analyze event rates and we include statistical aspects such that the results are directly applicable for the planning of optimal experimental setups. We discuss the capabilities of a neutrino-factory experiment as a function of the distance between the neutrino source and the detector and of the muon source energy for the optimal observation of the MSW effect. Moreover, we determine the sensitivity to the value of $\theta_{13}$ for different experimental configurations.

Demonstrating and testing the MSW effect directly is of fundamental importance since this effect plays a basic role in different neutrino physics scenarios. The MSW mechanism provides, for example, the only clue for understanding the solar neutrino deficit with a neutrino mass squared difference within a few orders of magnitude from that inferred from the atmospheric neutrino data. Atmospheric neutrinos can undergo matter-enhanced transitions in the earth. The matter effects in neutrino oscillations will play an important role in the interpretation of the results of a neutrino factory experiment using a $L \gtrsim 1000\,\mathrm{km}$ baseline. They also play a role in the searches for CP-violation in such experiments [2, 4], since matter effects generate an asymmetry between the two relevant CP-conjugated appearance channels [4]. Knowing the asymmetry caused by matter effects is therefore essential for obtaining information on the CP-violation originating from the lepton mixing matrix. Matter enhanced neutrino transitions can play important role in astrophysics as well.

Neutrino factories are extensively discussed in the literature [1, 2, 3, 5, 6, 7, 8]. Either muons or anti-muons are accelerated to an energy $E_\mu$ and decay then in straight sections of a storage ring like $\mu^- \to e^- + \bar{\nu}_e + \nu_\mu$ or $\mu^+ \to e^+ + \bar{\nu}_\mu + \nu_e$ so that a very pure neutrino beam containing $\bar{\nu}_e$ and $\nu_\mu$ or $\nu_e$ and $\bar{\nu}_\mu$, respectively, is produced. The muon energy $E_\mu$ could be in a wide range from 10 GeV to 50 GeV or more and a neutrino flux corresponding to $2 \cdot 10^{20}$ muon decays per year in the straight section of the ring pointing to a remote detector could be achieved. Higher fluxes are also currently under discussion [9]. The neutrino fluxes are

therefore very intense and can be easily calculated from the decay spectrum at rest. For unpolarized muons and negligible beam divergence one finds for a baseline of $L = 730$ km a neutrino flux of $\simeq 4.3 \cdot 10^{12}$ yr$^{-1}$m$^{-2}$ and for a baseline $L = 10000$ km a neutrino flux $\simeq 2.3 \cdot 10^{10}$ yr$^{-1}$m$^{-2}$. Note also that the $\bar{\nu}_e$ and $\nu_e$ fluxes depend sizably on the beam polarization, that will be assumed to be negligible in this paper. Altogether a neutrino factory would provide pure and high-intensity neutrino beams with a well known energy spectrum that in turn would allow a wide physical program including precise measurement of mixing parameters [2, 3], matter effects [5, 8] and, in case of LMA solution of the solar problem, leptonic CP-violation [6, 7].

The produced neutrino beam will be directed towards a remote detector at a given Nadir angle $h$, which corresponds to an oscillation baseline $L = 2R_\oplus \cos(h)$ , where $R_\oplus = 6371$ km is the earth radius. If $L \gtrsim 10^3$ km, as we shall assume, matter effects become important in neutrino oscillations[1]. For $L \leq 10600$ km the beam traverses the earth along a trajectory in the earth mantle without crossing the earth core where the density is substantially higher. According to the earth models [12, 13], the average matter density along the neutrino trajectories with $L = (10^3 - 10^4)$ km lies in the interval $\sim$ (2.9 - 4.8) g/cm$^3$. The matter density changes along each trajectory, but the variation is relatively small - by about 1.5 to 2.0 g/cm$^3$, and even the largest takes place over relatively big distances of several thousand kilometers. As a consequence, one can approximate the earth mantle density profile by a constant average density distribution. The constant density should be chosen to be equal to the average density along every trajectory [14, 15, 16]. For the calculation of the neutrino oscillation probabilities in the case of interest, the indicated constant density model provides a very good approximation to the somewhat more complicated density structure of the earth mantle (for a recent discussion see, e.g., [17]). Let us note also that the earth mantle is with a good precision isotopically symmetric: $Y_e = 0.494$ [12, 13], where $Y_e$ is the electron fraction number in the mantle.

Since the beam consists always either of $\nu_e$ together with $\bar{\nu}_\mu$ or $\bar{\nu}_e$ in combination with $\nu_\mu$ there are, in principle, eight different appearance experiments and four different disappearance experiments which could be performed[2]. From an experimental point of view, however, at present the four channels with muon neutrinos or antineutrinos in the final state, $\nu_\mu \to \nu_\mu$, $\bar{\nu}_\mu \to \bar{\nu}_\mu$, $\nu_e \to \nu_\mu$, $\bar{\nu}_e \to \bar{\nu}_\mu$ seem to be most promising. A very important issue is in this context the ability of the detector to discriminate between neutrinos and antineutrinos, namely the ability to measure the charge of the leptons produced by the neutrino charged current interactions. Note that very good discrimination capability is required for a measurement of the appearance probabilities since they produce "wrong sign" muon events in the detector and have to be discriminated from the much larger number of events associated with the $\nu_\mu$ and $\bar{\nu}_\mu$ survival probabilities. The channels with electron neutrinos or antineutrinos in the final state are problematic from this point of view due to the difficulty of telling $e^+$ from $e^-$ in a large high-density detector. On the contrary, a very good $\mu^+/\mu^-$ discrimination could be obtained in a large properly oriented magnetized detector [19].

[1] The possibility to detect matter effects in long baseline neutrino oscillation experiments with $L \simeq 730$ km (MINOS, CERN - GS) was discussed, e.g., in refs. [10, 11].

[2] For pre-neutrino factory discussions of very long baseline terrestrial neutrino oscillation experiments see, e.g., [18].

The paper is organized as follows. In section 2 we give the analytic formulae for three neutrino oscillations in matter which contain the essential physics relevant for our study. In the following section 3 we discuss event rates, their parameter dependence, their scaling behaviour and we show results from our numerical calculations. In section 4 we define the sensitivity to matter effects in a statistical sense and discuss the results of our numerical calculations including parameter uncertainties. This is followed by a discussion in section 5 of the effects of a non-vanishing $\Delta m^2_{21}$. In section 6 the possibility of detecting matter effects by looking for the characteristic enhancement, the broadening and the shift of the dominating maximum of the event rate energy spectrum is discussed and we conclude in section 7.

## 2 Three Neutrino Oscillation Probabilities in Matter

We will assume in this paper the existence of three flavour neutrino mixing:

$$|\nu_l > \;\; = \sum_{k=1}^{3} U_{lk} |\nu_k > \;\; , \qquad l = e, \mu, \tau, \tag{1}$$

where $|\nu_l >$ is the state vector of the (left-handed) flavour neutrino $\nu_l$, $|\nu_k >$ is the state vector of a neutrino $\nu_k$ possessing a definite mass $m_k$, $m_k \neq m_j$, $k \neq j = 1, 2, 3$ and $U$ is a $3 \times 3$ unitary matrix – the lepton mixing matrix. We conventionally order the masses in such a way that $0 < \Delta m^2_{21} < |\Delta m^2_{31}|$. According to the sign of $\Delta m^2_{31}$, the previous convention corresponds to the two closest neutrino masses ($m_1$,$m_2$) being lighter than the third one ($m_3$) ($m_3 > m_2 > m_1$ and $\Delta m^2_{31} > 0$) or being heavier than the third one ($m_2 \gtrsim m_1 > m_3$ and $\Delta m^2_{31} < 0$)[3]. As long as matter and CP-violation effects are not taken into account, the two cases are phenomenologically equivalent from the point of view of neutrino oscillations. It is natural to suppose in this case that one of the two independent neutrino mass-squared differences, say $\Delta m^2_{21}$, is relevant for the vacuum oscillation (VO), small or large mixing angle MSW solutions[4] (SMA MSW and LMA MSW) of the solar neutrino problem with values in the intervals [20, 21]

$$\text{VO}: \quad 5.0 \times 10^{-11}\,\text{eV}^2 \lesssim \Delta m^2_{21} \lesssim 5.0 \times 10^{-10}\,\text{eV}^2 \;, \tag{2a}$$

$$\text{SMA MSW}: \quad 4.0 \times 10^{-6}\,\text{eV}^2 \lesssim \Delta m^2_{21} \lesssim 9.0 \times 10^{-6}\,\text{eV}^2 \;, \tag{2b}$$

$$\text{LMA MSW}: \quad 2.0 \times 10^{-5}\,\text{eV}^2 \lesssim \Delta m^2_{21} \lesssim 2.0 \times 10^{-4}\,\text{eV}^2 \;, \tag{2c}$$

while $\Delta m^2_{31}$ is responsible for the dominant atmospheric $\nu_\mu \leftrightarrow \nu_\tau$ oscillations and lies in the interval

$$\text{ATM}: \quad 10^{-3}\,\text{eV}^2 \lesssim |\Delta m^2_{31}| \lesssim 8.0 \times 10^{-2}\,\text{eV}^2 \;. \tag{3}$$

[3]This scheme implies an approximate degeneracy of either $m_1$ and $m_2$ or of all the mass eigenstates.

[4]There exists also a large mixing angle solution of the solar neutrino problem with $\Delta m^2_{21} \sim 10^{-7}\,\text{eV}^2$ - the LOW solution, which, however, provides a somewhat worse description of the data than the MSW and the VO solutions [20].

For $E_\nu \geq 1\,\mathrm{GeV}$, $L \leq 10^4$ km, the $\Delta m^2$-hierarchy

$$\Delta m^2_{21} \ll |\Delta m^2_{31}| \tag{4}$$

and $\Delta m^2_{21} \ll 10^{-4}\,\mathrm{eV}^2$, the probabilities of three-neutrino oscillations in vacuum of interest reduce effectively to two-neutrino vacuum oscillation probabilities [22, 23]:

$$P^{3\nu}_{vac}(\nu_l \to \nu_{l'}) = P^{vac}(\bar\nu_l \to \bar\nu_{l'}) \cong 2|U_{l3}|^2|U_{l'3}|^2 \left(1 - \cos\frac{\Delta m^2_{31}L}{2E}\right),\ l \neq l' = e,\mu,\tau, \tag{5}$$

$$P^{3\nu}_{vac}(\nu_l \to \nu_l) = P^{3\nu}_{vac}(\bar\nu_l \to \bar\nu_l) \cong 1 - 2|U_{l3}|^2(1 - |U_{l3}|^2) \left(1 - \cos\frac{\Delta m^2_{31}L}{2E}\right),\ l = e,\mu,\tau. \tag{6}$$

Under the conditions (1) and (4) the element $|U_{e3}|$ of the lepton mixing matrix, which controls the $\nu_e \to \nu_{\mu(\tau)}$, $\bar\nu_e \to \bar\nu_{\mu(\tau)}$, $\nu_\mu \to \nu_e$ and the $\bar\nu_\mu \to \bar\nu_e$ oscillations, is tightly constrained by the CHOOZ experiment [24] and the oscillation interpretation of the solar and atmospheric neutrino data: for $3.0 \times 10^{-3}\,\mathrm{eV}^2 \leq \Delta m^2_{31} \leq 8.0 \times 10^{-3}\,\mathrm{eV}^2$ one has

$$|U_{e3}|^2 \lesssim 0.025\ . \tag{7}$$

The CHOOZ upper limit is less stringent for $1.0 \times 10^{-3}\,\mathrm{eV}^2 \leq |\Delta m^2_{31}| < 3.0 \times 10^{-3}\,\mathrm{eV}^2$ where values of $|U_{e3}|^2 \cong 0.05$ are allowed.

Note that under the condition (4), the VO or MSW transitions of solar neutrinos depend on $|U_{e3}|^2$ and on the two-neutrino VO or MSW transition probability with $\Delta m^2_{21}$ and $\theta_{12}$, where

$$\sin^2 2\theta_{12} = 4\frac{|U_{e1}|^2\ |U_{e2}|^2}{(|U_{e1}|^2 + |U_{e2}|^2)^2}, \quad \cos 2\theta_{12} = \frac{|U_{e1}|^2 - |U_{e2}|^2}{|U_{e1}|^2 + |U_{e2}|^2}\ , \tag{8}$$

playing the role of the corresponding two-neutrino oscillation parameters [25, 26, 27] (for recent reviews see, e.g., [28, 29]). For $|U_{e3}|^2$ satisfying the limit (7), however, this dependence is rather weak and cannot be used to further constrain or determine $|U_{e3}|^2$. In general, under the condition (4) and for $\Delta m^2_{21} \ll 10^{-4}\,\mathrm{eV}^2$ the relevant solar neutrino transition probability depends only on the absolute values of the elements of the first row of the lepton mixing matrix, i.e., on $|U_{ei}|^2$, i=1,2,3, while the oscillations of the (atmospheric) $\nu_\mu$, $\bar\nu_\mu$, $\nu_e$ and $\bar\nu_e$ on earth distances are controlled by the elements of the third column of $U$, $|U_{l3}|^2$, $l = e,\mu,\tau$. The other elements of $U$ are not accessible to direct experimental determination. Moreover, the $CP-$ and $T-$ violation effects in the oscillations of neutrinos are negligible.

For our analysis we use a standard parametrization of the lepton mixing matrix $U$:

$$\begin{pmatrix} U_{e1} & U_{e2} & U_{e3} \\ U_{\mu1} & U_{\mu2} & U_{\mu3} \\ U_{\tau1} & U_{\tau2} & U_{\tau3} \end{pmatrix} = \begin{pmatrix} c_{12}c_{13} & s_{12}c_{13} & s_{13}e^{-i\delta} \\ -s_{12}c_{23} - c_{12}s_{23}s_{13}e^{i\delta} & c_{12}c_{23} - s_{12}s_{23}s_{13}e^{i\delta} & s_{23}c_{13} \\ s_{12}s_{23} - c_{12}c_{23}s_{13}e^{i\delta} & -c_{12}s_{23} - s_{12}c_{23}s_{13}e^{i\delta} & c_{23}c_{13} \end{pmatrix} \tag{9}$$

where $c_{ij} \equiv \cos\theta_{ij}$, $s_{ij} \equiv \sin\theta_{ij}$ and $\delta$ is the Dirac CP-violation phase[5]. The angles $\theta_{12}$ and $\theta_{23}$ in (9) are constrained to lie within rather narrow intervals by the solar and atmospheric

[5]We have not written explicitly the possible Majorana CP-violation phases which do not enter into the expressions for the oscillation probabilities of interest [30]. Furthermore we assume throughout this study $0 \leq \theta_{12}, \theta_{23}, \theta_{13} < \pi/2,\ 0 \leq \delta < 2\pi$.

neutrino data for each of the different solutions, eqs. (2a) - (2c), of the solar neutrino problem. With the accumulation of data the uncertainties in the knowledge of $\theta_{12}$ and $\theta_{23}$ will diminish, while only upper limits on $s^2_{13}$ like eq. (7) have been obtained so far. The mixing angle $\theta_{13}$ is one of the 4 (or 6 - depending on whether the massive neutrinos are of Dirac or Majorana type [30, 23]) fundamental parameters in the lepton mixing matrix. It controls the probabilities of the $\nu_\mu(\nu_e) \to \nu_e(\nu_\mu)$, $\bar{\nu}_\mu(\bar{\nu}_e) \to \bar{\nu}_e(\bar{\nu}_\mu)$, $\nu_e \to \nu_\tau$ and $\bar{\nu}_e \to \bar{\nu}_\tau$ oscillations and the $CP-$ and $T-$violation effects in neutrino oscillations depends on it. Obviously, one of the main goals of the future neutrino oscillation experiments should be to determine the value of $\theta_{13}$ or to obtain a more stringent experimental upper limit than the existing one (9).

Under the condition (4), with $\Delta m^2_{21} \ll 10^{-4}\,\mathrm{eV}^2$ and in constant density approximation, the oscillation probabilities of interest take the following simple form (see, e.g., [26, 31, 29]):

$$P^{3\nu}_E(\nu_\mu \to \nu_e) = P^{3\nu}_E(\nu_e \to \nu_\mu) \cong s^2_{23}\; P^{2\nu}_E(\Delta m^2_{31}, \sin^2 2\theta_{13})\;, \tag{10a}$$

$$\begin{aligned} P^{3\nu}_E(\nu_\mu \to \nu_\mu) \cong\; & c^4_{23} + s^4_{23}\left[1 - P^{2\nu}_E(\Delta m^2_{31}, \sin^2 2\theta_{13})\right] \\ & + 2c^2_{23}s^2_{23}\;\left[\cos\kappa - (1+\cos 2\theta^m_{13})\;\sin\frac{\Delta E_m L}{2}\;\sin(\kappa + \frac{\Delta E_m L}{2})\right]\;, \end{aligned} \tag{10b}$$

$$\begin{aligned} P^{3\nu}_E(\nu_\mu \to \nu_\tau) \cong\; & 2c^2_{23}s^2_{23}\;\left[2\sin^2\frac{\kappa}{2} - \frac{1}{2}P^{2\nu}_E(\Delta m^2_{31}, \sin^2 2\theta_{13})\right. \\ & \left. + (1+\cos 2\theta^m_{13})\;\sin\frac{\Delta E_m L}{2}\;\sin(\kappa + \frac{\Delta E_m L}{2})\right]\;, \end{aligned} \tag{10c}$$

where

$$P^{2\nu}_E(\Delta m^2_{31}, \sin^2 2\theta_{13}) = \frac{1}{2}\left[1 - \cos\Delta E_m L\right]\sin^2 2\theta^m_{13} \tag{11}$$

is the two-neutrino transition probability in matter with constant density and

$$\kappa \cong \frac{L}{2}\;\left[\frac{\Delta m^2_{31}}{2E} + V - \Delta E_m\right] \tag{12}$$

is a phase. In eqs. (11) - (12), $\Delta E_m$ and $\theta^m_{13}$ are the neutrino energy difference and mixing angle in matter,

$$\Delta E_m = \frac{|\Delta m^2_{31}|}{2E}C_+, \quad \cos 2\theta^m_{13} = \frac{1}{C_+}\left(\cos 2\theta_{13} - \frac{2EV}{\Delta m^2_{31}}\right)\;, \tag{13}$$

where

$$C^2_\pm = \left(1 \mp \frac{2EV}{\Delta m^2_{31}}\right)^2 \pm 4\frac{2EV}{\Delta m^2_{31}}\sin^2\theta_{13} \tag{14}$$

and

$$V = \sqrt{2}G_F\bar{N}^{man}_e \tag{15}$$

is the matter term, $\bar{N}_e^{man}$ being the average electron number density along the neutrino trajectory in the earth mantle, The probability $P_E^{3\nu}(\nu_e \to \nu_\tau)$ can be obtained from eq. (10a) by replacing the factor $s^2_{23}$ with $c^2_{23}$. The corresponding antineutrino transition and survival probabilities have the same form and can formally be obtained from eqs. (10a–10c) by changing the sign of the matter term, i.e. $\bar{N}_e^{man} \to -\bar{N}_e^{man}$ in the expressions for $\kappa$, $\Delta E_m \cos 2\theta^m_{13}$, eqs. (12)–(13), and by replacing $C_+$ by $C_-$. Expressions (10) follow directly from eqs. (12), (13b), (14b) and eq. (19) in [26] (after setting in the corresponding formulae $\varphi'_{23} = 0$, $\varphi'_{12} = \pi/2$). They can be deduced also from the explicit expressions for the probabilities of neutrino oscillations of the earth-core-crossing neutrinos in the two-layer approximation for the earth density distribution (see, e.g., [14, 15, 16, 32]), obtained in [31] (on the basis of [26]) and in [33].

As we shall see in Section 5, at distances $L \lesssim 6000$ km and for $\Delta m^2_{21} \sim 10^{-4}$ eV$^2$, the $\Delta m^2_{21}$ corrections in the probabilities of interest $P_E^{3\nu}(\nu_\mu \to \nu_e)$, $P_E^{3\nu}(\nu_\mu \to \nu_\mu)$ and $P_E^{3\nu}(\nu_\mu \to \nu_\tau)$ can be non-negligible. Utilizing the results of [26] it is not difficult to derive also the expressions for these probabilities including the leading order (CP-conserving and CP-violating) $\Delta m^2_{21}$-corrections [34]. One finds in the case of the probability $P_E^{3\nu}(\nu_e \to \nu_\mu)$:

$$
\begin{aligned}
P_E^{3\nu}(\nu_e \to \nu_\mu) \cong\; & s^2_{23}\,[1 + \cos\delta \cot\theta_{23} \sin 2\theta'_{23}]\; P_E^{2\nu}(\,\overline{\Delta m}^2_{31}, \theta_{13}) \\
& + \;\; \cos\theta'_{12}\;\; \sin 2\theta_{23}\;\; \sin 2\bar{\theta}^m_{13}\;\; \sin\frac{\Delta\bar{E}_m L}{2} \\
& \times \;\; \left[\cos\delta\left(\sin(\bar{\kappa} + \frac{\Delta\bar{E}_m L}{2}) - \cos 2\bar{\theta}^m_{13}\sin\frac{\Delta\bar{E}_m L}{2}\right)\right. \\
& \left. - \; 2\sin\delta\;\; \sin\frac{\bar{\kappa}}{2}\;\; \sin(\frac{\bar{\kappa}}{2} + \frac{\Delta\bar{E}_m L}{2})\right]\;, \qquad (16)
\end{aligned}
$$

where [26, 34]

$$
\overline{\Delta m}^2_{31} \equiv \Delta m^2_{31} - s^2_{12}\Delta m^2_{21}\;, \qquad (17)
$$

$$
\bar{\kappa} = \frac{L}{2}\;\left[\frac{\overline{\Delta m}^2_{31}}{2E} + V - \Delta\bar{E}_m\right] - \frac{L\Delta m^2_{21}}{2E}\cos 2\theta_{12} \qquad (18)
$$

and

$$
\cos\theta'_{12} = \frac{\Delta m^2_{21} c_{12} s_{12} c_{13}}{2EV + s^2_{13}\;\overline{\Delta m}^2_{31} - \Delta m^2_{21}\cos 2\theta_{12}} \cong \frac{\Delta m^2_{21} c_{12} s_{12} c_{13}}{2EV + s^2_{13}\;\Delta m^2_{31}}\;, \qquad (19)
$$

$$
\sin 2\theta'_{23} = -\;\frac{\Delta m^2_{21} s_{13}\sin 2\theta_{12}}{\overline{\Delta m}^2_{31} c^2_{13} - \Delta m^2_{21}\cos 2\theta_{12}} \cong -\;\frac{\Delta m^2_{21}}{\Delta m^2_{31}}\; s_{13}\sin 2\theta_{12}\;. \qquad (20)
$$

The expressions for $P_E^{2\nu}(\,\overline{\Delta m}^2_{31}, \theta_{13})$, $\Delta\bar{E}_m$ and $\cos 2\bar{\theta}^m_{13}$ are given by eqs. (11) and (13) in which $\Delta m^2_{31}$ is replaced by $\overline{\Delta m}^2_{31}$. The probability $P_E^{3\nu}(\bar{\nu}_e \to \bar{\nu}_\mu)$ ($P_E^{3\nu}(\nu_\mu \to \nu_e)$) can

be obtain from eq. (16) by making the change $V \to -V$ and $\delta \to -\delta$ ($\delta \to -\delta$). The expression (16) was obtained by neglecting the $\sim (\cos\theta'_{12})^2$, $(\sin 2\theta'_{23})^2$, $\cos\theta'_{12}\sin 2\theta'_{23}$ and the higher order corrections (for further details see [26, 34]). Note that if $\Delta m^2_{21} \leq 2\times 10^{-4}$ eV$^2$ and for $\bar{N}^{man}_e \gtrsim 1.45$ cm$^{-3}$N$_{\rm A}$ ($L \geq 1000$ km), we have $2EV \geq 10^{-3}\ eV^2$, and consequently $|\cos\theta'_{12}| \leq 0.1$ at $E \gtrsim 4.5$ GeV. For the indicated maximal value of $\Delta m^2_{21}$ and $|\Delta m^2_{31}| \geq 10^{-3}$ eV$^2$, $s^2_{13} \lesssim 0.025$ (0.05) one finds $|\sin 2\theta'_{23}| \lesssim 0.032$ (0.045). It follows from the preceding discussion that if $|\Delta m^2_{31}| \cong 3.5\times 10^{-3}$ eV$^2$, the correction $\sim \cos\theta'_{12}$ would be the dominant one for $E \sim (5-30)$ GeV. For the values of $\Delta m^2_{31}$ and $\Delta m^2_{21}$ of interest, the $\Delta m^2_{21}-$correction included in $\overline{\Delta m}^2_{31}$, eq. (17), essentially just shifts the resonance energy by at most $\sim 10\%$. The terms with the factors $\cos\delta$ and $\sin\delta$ in eq. (16) include the leading order CP-conserving and CP-violating $\Delta m^2_{21}-$corrections, associated with the phase $\delta$.

Several comments are in order. First, the analytic expressions eqs. (10a)–(10c) represent excellent approximations in the case of the VO and SMA MSW solutions of the solar neutrino problem and for values of $\Delta m^2_{21} \lesssim 5\times 10^{-5}$ eV$^2$ from the LMA MSW solution region. For $5\times 10^{-5}$ eV$^2 < \Delta m^2_{21} \lesssim 2\times 10^{-4}$ eV$^2$, the corrections due to $\Delta m^2_{21}$ can be non-negligible and we are going to discuss them in section 5. Second, as it is clear from eqs. (10a) and (11), the probabilities $P^{3\nu}_E(\nu_e \to \nu_\mu)$ and $P^{3\nu}_E(\bar\nu_e \to \bar\nu_\mu)$ cannot exceed $s^2_{23} \sim 0.5$. The maximal value $s^2_{23}$ can be reached only if the MSW resonance condition $\sin^2 2\theta^m_{13} = 1$ and the condition $\cos\Delta E_m L = -1$ are simultaneously fulfilled. At the MSW resonance, however, one has $\Delta E^{res}_m \cong 1.23\pi\times 10^{-4}$ km$^{-1}$ $\tan 2\theta_{13}\bar{N}^{man}_e[N_A{\rm cm}^{-3}]$, where $\bar{N}^{man}_e$ is in units of $N_A{\rm cm}^{-3}$, $N_A$ being the Avogadro number, and for $s^2_{13} \leq 0.025$ the second condition $\cos\Delta E^{res}_m L = -1$ can only be satisfied for $L \geq 10^4$ km. If $s^2_{13} = 0.05$ this condition requires $L \geq 8\times 10^3$ km. Given the fact that the neutrino fluxes decrease with the distance as $L^{-2}$, the above discussion suggests that the maximum of the event distribution in $E$ and $L$ in the transition $\nu_e \to \nu_\mu$ should take place approximately at the MSW resonance energy, but at values of $L$ smaller than those at which $max\,(P^{3\nu}_E(\nu_e \to \nu_\mu)) \cong s^2_{23}$. The MSW resonance energy is given by: $E_{\rm res} \cong 6.56 \times \Delta m^2_{31}[10^{-3}\,{\rm eV}^2]\cos 2\theta_{13}(\bar{N}^{man}_e[cm^{-3}N_A])^{-1}$ GeV, where $\Delta m^2_{31}$ is in units of $10^{-3}\,{\rm eV}^2$. For $\Delta m^2_{31}[10^{-3}\,{\rm eV}^2] = 3.5; 6.0, 8.0$ and, e.g., $\bar{N}^{man}_e[cm^{-3}N_A] = 2$, we have $E_{\rm res} \cong 11.5; 19.7; 26.2\cos 2\theta_{13}$ GeV. The $\nu_e \to \nu_\mu$ and $\bar\nu_e \to \bar\nu_\mu$ oscillations will be affected substantially by the MSW effect if the energy of the parent muon beam $E_\mu > E_{\rm res}$. This condition can be satisfied for any value of $\Delta m^2_{31}$ from the interval (3) for $E_\mu \gtrsim 30\,{\rm GeV}$. For the value of $\Delta m^2_{31}[10^{-3}\,{\rm eV}^2] = 3.5$ which is currently "preferred" by the Super-Kamiokande data we have $E_\mu \gtrsim 15\,{\rm GeV}$. Note that a change in the sign of $\Delta m^2_{31}$ reverses the sign of $N^{res}_e$ which opens the possibility to determine this sign via matter effects, as was noticed recently also in ref. [8]. The probabilities (10) for $L = 7330$ km (the Fermilab - Gran Sasso distance) have been discussed recently in [17].

## 3 Event Rates

We discuss now the effects of matter on the total rate of $\nu_e \to \nu_\mu$, $\bar\nu_e \to \bar\nu_\mu$, $\nu_\mu \to \nu_\mu$, $\bar\nu_\mu \to \bar\nu_\mu$ events. If, for example, $\mu^+$ are accumulated in the storage ring, the neutrino beam contains $\nu_e$ and $\bar\nu_\mu$. Since the neutrino-antineutrino transitions have a negligible rate, the beam-induced $\mu^+$ events in the detector must be attributed in this case to the charged current interactions of unoscillated $\bar\nu_\mu$. The total number $n_{\mu^+}(\mu^+)$ of $\mu^+$ events measures therefore an

averaged $\bar{\nu}_\mu$ survival probability. Wrong sign $\mu^-$ events must be attributed to $\nu_\mu$ generated by oscillations of the initial $\nu_e$, so that their total number $n_{\mu^+}(\mu^-)$ measures the averaged $\nu_e \to \nu_\mu$ oscillation probability. Analogously, for $\mu^-$ in the storage ring, the total numbers of $\mu^-$ and $\mu^+$ events $n_{\mu^-}(\mu^-)$, $n_{\mu^-}(\mu^+)$ measure the averaged $\nu_\mu$ survival probability and $\bar{\nu}_e \to \bar{\nu}_\mu$ oscillation probability, respectively.

The total number of events in each channel are given by

$$n_{\mu^+}(\mu^-) = N_{\mu^+} N_{\rm kT} \frac{10^9 N_A}{m_\mu^2 \pi} \frac{E_\mu^3}{L^2} \int_{E_{\rm min}}^{E_\mu} f_{\nu_e\nu_\mu}(E) P_E^{3\nu(\nu_e \to \nu_\mu)}(E) \, (dE/E_\mu) \ , \tag{21a}$$

$$n_{\mu^-}(\mu^+) = N_{\mu^-} N_{\rm kT} \frac{10^9 N_A}{m_\mu^2 \pi} \frac{E_\mu^3}{L^2} \int_{E_{\rm min}}^{E_\mu} f_{\bar{\nu}_e\bar{\nu}_\mu}(E) P_E^{3\nu(\bar{\nu}_e \to \bar{\nu}_\mu)}(E) \, (dE/E_\mu) \ , \tag{21b}$$

$$n_{\mu^-}(\mu^-) = N_{\mu^+} N_{\rm kT} \frac{10^9 N_A}{m_\mu^2 \pi} \frac{E_\mu^3}{L^2} \int_{E_{\rm min}}^{E_\mu} f_{\nu_\mu\nu_\mu}(E) P_E^{3\nu(\nu_\mu \to \nu_\mu)}(E) \, (dE/E_\mu) \ , \tag{21c}$$

$$n_{\mu^+}(\mu^+) = N_{\mu^-} N_{\rm kT} \frac{10^9 N_A}{m_\mu^2 \pi} \frac{E_\mu^3}{L^2} \int_{E_{\rm min}}^{E_\mu} f_{\bar{\nu}_\mu\bar{\nu}_\mu}(E) P_E^{3\nu(\bar{\nu}_\mu \to \bar{\nu}_\mu)}(E) \, (dE/E_\mu) \ , \tag{21d}$$

where $P_E^{3\nu}$ denotes the oscillation probability described in section 2, $N_{\mu^+}$ ($N_{\mu^-}$) is the number of "useful" $\mu^+$ ($\mu^-$) decays, namely the number of decays occurring in the straight section of the storage ring pointing to the detector, $N_{\rm kT}$ is the size of the detector in kilotons, $10^9 N_A$ is the number of nucleons in a kiloton, $E_\mu$ is the energy of the muons in the ring and $E_{\rm min} = 3\,{\rm GeV}$ is a lower cut on the neutrino energies that helps a good detection efficiency. Since low energy events are suppressed by the low initial flux and the low cross section (see below), the results do not depend significantly on the precise value of $E_{\rm min}$ for $E_{\rm min} < 5\,{\rm GeV}$. The functions $f$ averaging the probabilities are given by

$$f_{\nu_e\nu_\mu}(E) = g_{\nu_e}(E/E_\mu)(\sigma_{\nu_\mu}(E)/E_\mu)\epsilon_{\mu^-}(E) \ , \tag{22a}$$

$$f_{\bar{\nu}_e\bar{\nu}_\mu}(E) = g_{\bar{\nu}_e}(E/E_\mu)(\sigma_{\bar{\nu}_\mu}(E)/E_\mu)\epsilon_{\mu^+}(E) \ , \tag{22b}$$

$$f_{\nu_\mu\nu_\mu}(E) = g_{\nu_\mu}(E/E_\mu)(\sigma_{\nu_\mu}(E)/E_\mu)\epsilon_{\mu^-}(E) \ , \tag{22c}$$

$$f_{\bar{\nu}_\mu\bar{\nu}_\mu}(E) = g_{\bar{\nu}_\mu}(E/E_\mu)(\sigma_{\bar{\nu}_\mu}(E)/E_\mu)\epsilon_{\mu^+}(E) \tag{22d}$$

and take into account the appropriately normalized initial spectrum of $\nu$-neutrinos produced in the decay of unpolarized muons, $g_\nu(E/E_\mu)$, the charged current cross section per nucleon, $\sigma_{\nu_\mu(\bar{\nu}_\mu)}(E)$, and the efficiency for the detection of $\mu^-$ ($\mu^+$), $\epsilon_{\mu^-(\mu^+)}(E)$ (we neglect here the finite resolution of the detector). For the numerical calculations we use

$$g_{\nu_e}(x) = g_{\bar{\nu}_e}(x) = 12x^2(1-x) \ , \qquad g_{\nu_\mu}(x) = g_{\bar{\nu}_\mu}(x) = 2x^2(3-2x) \ , \tag{23a}$$

$$\sigma_{\nu_\mu}(E) = 0.67 \cdot 10^{-38} E\,{\rm cm}^2/{\rm GeV} \ , \qquad \sigma_{\bar{\nu}_\mu}(E) = 0.34 \cdot 10^{-38} E\,{\rm cm}^2/{\rm GeV} \tag{23b}$$

and $\epsilon_{\mu^-}(E) = \epsilon_{\mu^+}(E) = \epsilon$ for $E > E_{\rm min}$ so that $f_{\nu_e\nu_\mu}(E)/f_{\bar{\nu}_e\bar{\nu}_\mu}(E) = f_{\nu_\mu\nu_\mu}(E)/f_{\bar{\nu}_\mu\bar{\nu}_\mu}(E) = 2$ independently of the energy.

The contribution of the background to the number of muons observed in the detector has been neglected in eqs. (21). That background includes muons from the decay of charm

quarks produced by charged and neutral current neutrino interactions in the detector and from the decay of $\tau$ produced by $\nu_\tau$ interactions. Both these sources can be kept under control in different ways [35, 8]. Let us note also that in eqs. (21) the possible divergence of the muon beam in the straight section of the storage ring has been neglected.

We can analyze now the dependence of $n_{\mu^+}(\mu^-)$, $n_{\mu^-}(\mu^+)$, $n_{\mu^-}(\mu^-)$, $n_{\mu^+}(\mu^+)$ on the mixing angles, the CP-phase $\delta$ and some of the experimental parameters. In the $\Delta m^2_{12} \ll 10^{-4}\,\mathrm{eV}^2$ approximation discussed above, the only relevant mixing angles are $\theta_{23}$ and $\theta_{13}$. In the leading order in a $\theta_{13}$ expansion the dependence of the total event rates in matter (and in vacuum) on these parameters is

$$n_{\mu^-}(\mu^-), n_{\mu^+}(\mu^+) \propto \sin^2 2\theta_{23}\ , \tag{24a}$$

$$n_{\mu^+}(\mu^-), n_{\mu^-}(\mu^+) \propto \sin^2\theta_{23} \sin^2 2\theta_{13}\ . \tag{24b}$$

Higher order corrections in $\theta_{13}$ are constrained by the CHOOZ limit. Despite the resonant matter enhancement of the mixing due to $\theta_{13}$, such corrections become only sizable for $\theta_{13}$ close to its upper limit and very long baselines where they can reach about 20% in the resonance channels.

Since eq. (24b) will turn out to be useful when discussing the sensitivity to matter effects, we discuss it in greater detail. Let us write eqs. (10a) in the form

$$P^{3\nu}_E(\nu_e \to \nu_\mu, \bar\nu_e \to \bar\nu_\mu) = \sin^2\theta_{23} \sin^2 2\theta_{13} \left(\frac{\sin(\Delta_{31} C_\pm)}{C_\pm}\right)^2 , \tag{25}$$

where $C_+$ is given by eq. (14) and corresponds to neutrinos, $C_-$ to antineutrinos and $\Delta_{31} = \Delta m^2_{31} L/(4E)$. Note that $C_+$ enhances the rates when $\Delta m^2_{31} > 0$, depletes them when $\Delta m^2_{31} < 0$. Therefore the sign of $\Delta m^2_{31}$ determines whether the enhanced channel is the neutrino or the antineutrino one. In the limit in which $\sin^2\theta_{13}$ can be neglected on the right-hand side of eq. (14), eq. (25) shows that $n_{\mu^+}(\mu^-)$, $n_{\mu^-}(\mu^+)$ are indeed proportional to $\sin^2 2\theta_{13}$. Despite the CHOOZ limit, $\sin^2\theta_{13} \lesssim 0.025$, the second term in eq. (14) can be relevant when the first term vanishes around the resonance. For $2EV = \Delta m^2_{31}$ we have in fact $C_+ = 2\sin\theta_{13}$ and

$$P^{3\nu}_E(\nu_e \to \nu_\mu) = \sin^2\theta_{23} \sin^2 2\theta_{13}\, \frac{L^2V^2}{4} \left(\frac{\sin(\sin\theta_{13} LV)}{\sin\theta_{13} LV}\right)^2 , \tag{26}$$

whereas by neglecting the $\sin^2\theta_{13}$ term in (14) we would get $C_+ = 0$ and

$$P^{3\nu}_E(\nu_e \to \nu_\mu) = \sin^2\theta_{23} \sin^2 2\theta_{13}\, \frac{L^2V^2}{4}\ . \tag{27}$$

A comparison of eqs. (26) and (27) shows however that this approximation works even at the resonance provided $L \lesssim \pi/(4V\sin\theta_{13}) \sim 7000\,\mathrm{km}\,(0.15/\sin\theta_{13})$. The effect of the $\sin^2\theta_{13}$ term in eq. (14) is therefore maximal in eq. (14) for very long baselines and $\theta_{13}$ close to the experimental limit. In this case it can affect the rates sizably, while it is negligible for smaller $\theta_{13}$ or smaller baseline. For a better approximation one can use, for muon energies such that the main contribution to the rates comes from neutrinos at the resonance,

$$n_{\mu^+}(\mu^-), n_{\mu^-}(\mu^+) \propto \sin^2\theta_{23} \sin^2 2\theta_{13} \left(\frac{\sin(\sin\theta_{13} LV)}{\sin\theta_{13} LV}\right)^2 , \tag{28}$$

which deviates less than 5% from the exact result in the whole parameter space ($L \lesssim 10000\,\text{km}$, $20\,\text{GeV} \lesssim E_\mu \lesssim 50\,\text{GeV}$). In most cases $L \lesssim \pi/(4V\sin\theta_{13})$ holds and the oscillating term in eq. (28) can be expanded, giving eqs. (24) or higher order approximations. We stress that in eq. (28) the baseline $L$ appears as part of the correction to the $\theta_{13}$, $\theta_{23}$ scaling only. The dependence on $L$ of the rates is more involved, especially for very large baselines, and will be described in figs. 1, 2. Note that the dependence on the beam intensity, detector size and efficiency is trivial:

$$n_{\mu^+}(\mu^-), n_{\mu^-}(\mu^-) \propto N_{\mu^+} N_{\text{kT}}\, \epsilon_{\mu^+}\ , \tag{29a}$$

$$n_{\mu^-}(\mu^+), n_{\mu^+}(\mu^+) \propto N_{\mu^-} N_{\text{kT}}\, \epsilon_{\mu^-}\ . \tag{29b}$$

We present now quantitative results for the total rates in matter for $\Delta m^2_{21} \ll 10^{-4}\,\text{eV}^2$ and we compare them with the results one would obtain in vacuum. The statistical significance of the matter effects will be discussed in the following section and effects of larger $\Delta m^2_{21}$ will be covered in section 5.

The total event rates depend, as already discussed, in a transparent way on the experimental parameters $N_{\mu^\pm}$, $N_{\text{kT}}$, $\epsilon_{\mu^\pm}$ and on the mixing parameters $\theta_{23}$, $\theta_{13}$. We focus our discussion therefore on the less transparent dependence on the baseline and muon energy. For that we use the central value of $\Delta m^2_{31} = 3.5 \cdot 10^{-3}\,\text{eV}^2$, and we assume $\Delta m^2_{31} > 0$. In the $\Delta m^2_{21} \ll 10^{-4}\,\text{eV}^2$ approximation, in which CP-violation effects are negligible, the results for $\Delta m^2_{31} < 0$ can be obtained by simply interchanging neutrinos and antineutrinos.

The total number of events in the two appearance channels $\nu_e \to \nu_\mu$, $\bar\nu_e \to \bar\nu_\mu$ is shown for $E_\mu = 20\,\text{GeV}$ and $E_\mu = 50\,\text{GeV}$ in fig. 1 as a function of the baseline (solid lines) in comparison with the event rates one would get if the neutrinos did not interact with matter (dashed lines). Fig. 2 shows the same results for the two disappearance channels $\nu_\mu \to \nu_\mu$, $\bar\nu_\mu \to \bar\nu_\mu$. Both figures correspond to a "default" experimental set-up providing $N_{\mu^+} = N_{\mu^-} = N_\mu = 2 \cdot 10^{20}$ useful muon decays (e.g. in one year of running) and to a detector with $N_{\text{kT}} = 10$ kilotons and an efficiency $\epsilon_{\mu^+} = \epsilon_{\mu^-} = \epsilon = 50\%$ in both channels. The rates depend only on the combination $N_\mu N_{\text{kT}} \epsilon$ which is in our case $N_\mu N_{\text{kT}} \epsilon = 10^{21}$. We assume for these figures that $\sin^2 2\theta_{23} = 1$ and $\sin^2 2\theta_{13} = 0.01$, one order of magnitude below the experimental limit. The rates for different values of $N_\mu$, $N_{\text{kT}}$, $\epsilon$, $\theta_{23}$, $\theta_{13}$ can be obtained by using eqs. (29), (24a) and (24b) or (28).

The vacuum event rates in the neutrino channels are twice as big as the rates in the antineutrino channels. This is because the oscillation probabilities are in the CP-conjugated channels in the $\Delta m^2_{21} \ll 10^{-4}\,\text{eV}^2$ approximation the same while the functions averaging the probabilities are larger by a factor 2 in the neutrino channels (due to the larger cross-section). The disappearance channels shown in fig. 2 are essentially independent of matter effects since these effects come only with the $\theta_{13}$ corrections to the oscillation probabilities[6]. In contrast, fig. 1 shows the drastic enhancement (depletion) of the event rates in the $\nu_e \to \nu_\mu$ ($\bar\nu_e \to \bar\nu_\mu$) channel for very long baselines. The growth of the total rates with the muon energy which is obvious from eqs. (21) can also be seen in fig. 1.

[6] As discussed above effects as large as 20% can occur for $\theta_{13}$ close to the CHOOZ limit and very large baselines.

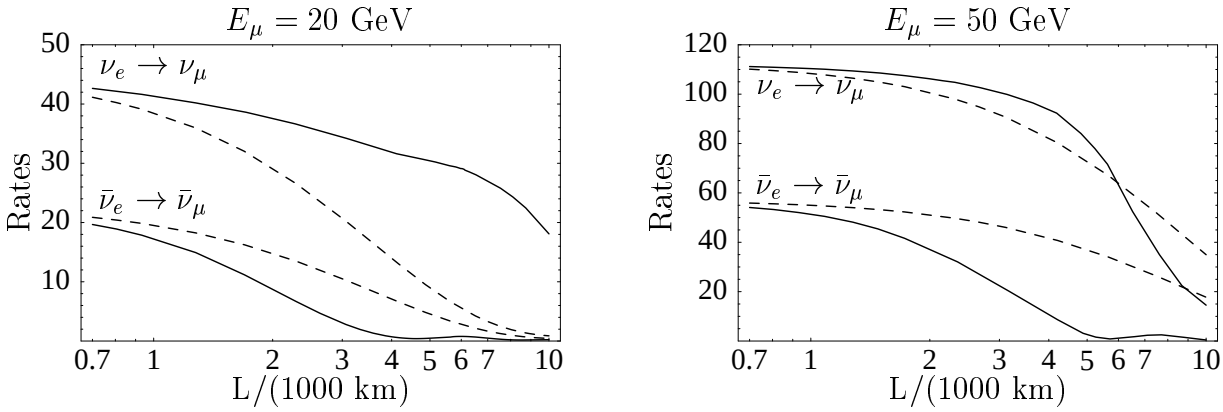


**Figure 1**: *Appearance event rates $n_{\mu^+}(\mu^-)$, $n_{\mu^-}(\mu^+)$ due to the $\nu_e \to \nu_\mu$ and $\bar{\nu}_e \to \bar{\nu}_\mu$ transitions in the earth mantle (solid lines) and in vacuum (dashed lines), as functions of the baseline L for $E_\mu = 20\,\mathrm{GeV}$ (left) and $E_\mu = 50\,\mathrm{GeV}$ (right). The differences between the solid and dashed lines is a measure of the magnitude of the earth matter effect. Both plots assume $N_\mu = 2 \cdot 10^{20}$, $\epsilon = 50\%$, $\sin^2 2\theta_{23} = 1$ and $\sin^2 2\theta_{13} = 0.01$. The scaling of the rates with these parameters is described in the text.*

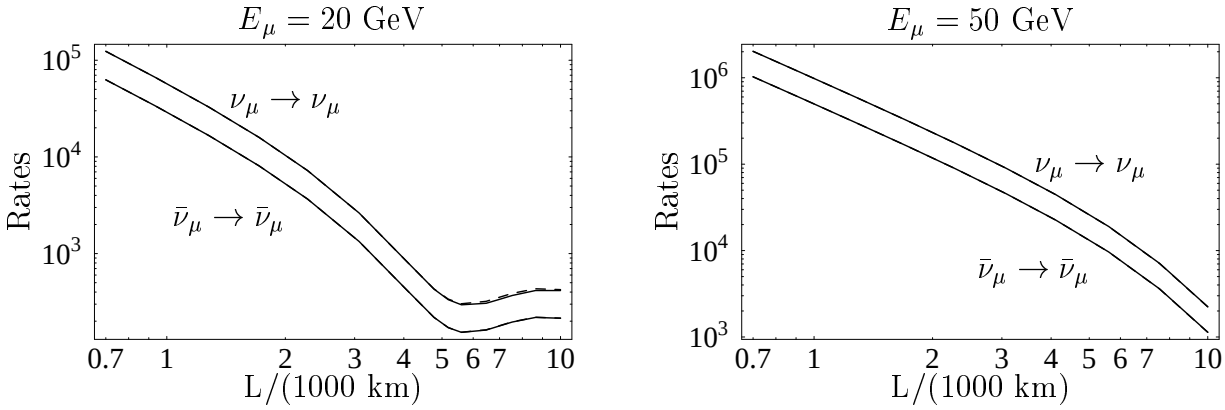


**Figure 2**: *Same as in fig. 1 but for the disappearance channels. The dashed lines coincide almost perfectly with the solid lines, showing that matter effects are negligible in these channels.*

Figs. 3 and 4 show in more detail the differential event rates of the appearance channels $\nu_e \to \nu_\mu$ and $\bar{\nu}_e \to \bar{\nu}_\mu$ as three dimensional plots over $L$ and $E_\nu$. The figures show nicely the enhancement (suppression) due to the MSW mechanism in the $\nu_e \to \nu_\mu$ ($\bar{\nu}_e \to \bar{\nu}_\mu$) channel for large baseline $L$. To understand these figures we can look at the values of $dn_{\mu^+}(\mu^-)/dE$ and $dn_{\mu^-}(\mu^+)/dE$ for three different energies, $E = (5;\ 10;\ 15)\,\mathrm{GeV}$, and two baselines $L$. Specifically we compare a relatively short baseline $L = L_0 \equiv 1000$ km with a long baseline $L = 6000$ km where matter effects are more important. For $L = 1000$ km ($L = 6000$ km) the average matter electron density is $\bar{N}_e^{man} = 1.45\ \mathrm{cm}^{-3}\mathrm{N_A}$ ($\bar{N}_e^{man} \cong 2.0\ \mathrm{cm}^{-3}\mathrm{N_A}$), resulting in a resonance neutrino energy of $E_{res} = 15.8\,\mathrm{GeV}$ ($E_{res} = 11.5\,\mathrm{GeV}$). The resonance energy is thus only somewhat reduced for larger baselines. The corresponding values of $\Delta_{31}(L) \equiv$

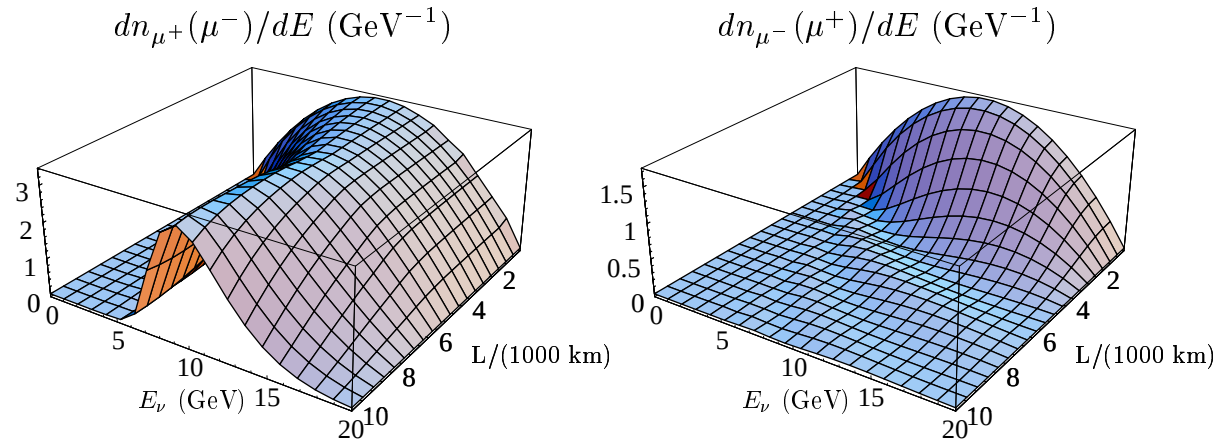


**Figure 3**: *Differential appearance rates for the channels $\nu_e \to \nu_\mu$ (left) and $\bar{\nu}_e \to \bar{\nu}_\mu$ (right) as functions of L and E for the same values of the parameters for which fig. 1 was obtained. The asymmetry, i.e. the enhancement of $dn_{\mu^+}(\mu^-)/dE$ and the suppression of $dn_{\mu^-}(\mu^+)/dE$, at $L \gtrsim (5000 - 6000)$km is related to the MSW effect (see the text).*

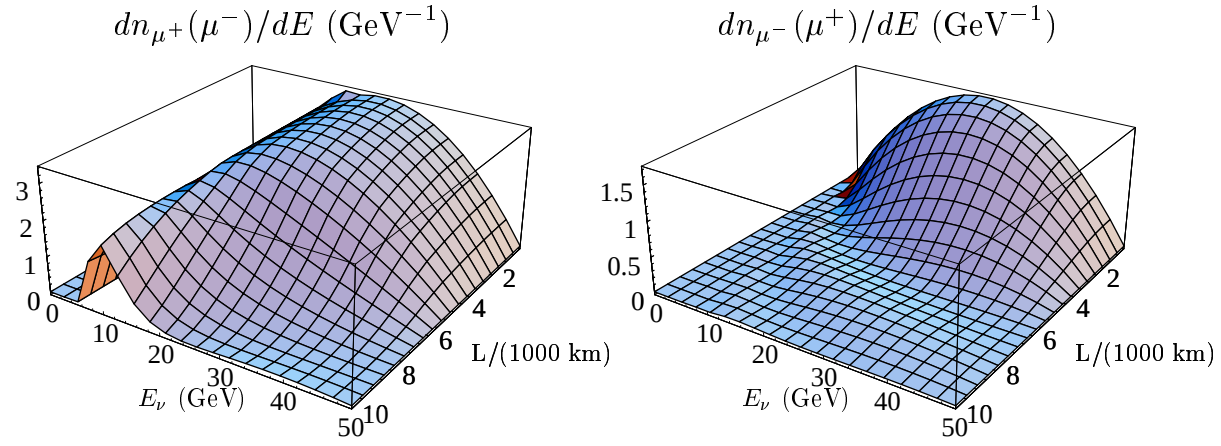


**Figure 4**: *Same as in fig. 3 but for a beam energy of* 50 GeV.

$L\ \Delta m^2_{31}/(4E)$ and the matter effect factors $C_+$ and $C_-$ which enter in $P^{3\nu}_E(\nu_e \to \nu_\mu)$ and $P^{3\nu}_E(\bar\nu_e \to \bar\nu_\mu)$ (see eqs. (10), (11), (13) and (14)) are displayed in Table 1.

| $L$ | 1000km | | | 6000km | | |
|---|---|---|---|---|---|---|
| $E$ | 5 GeV | 10 GeV | 15 GeV | 5 GeV | 10 GeV | 15 GeV |
| $\Delta_{31}(L)$ | $0.282\pi$ | $0.141\pi$ | $0.094\pi$ | $1.694\pi$ | $0.847\pi$ | $0.565\pi$ |
| $C_+$ | 0.686 | 0.371 | 0.111 | 0.568 | 0.159 | 0.327 |
| $C_-$ | 1.315 | 1.630 | 1.945 | 1.434 | 1.869 | 2.304 |
| $\Delta_{31}(L)C_+$ | 0.610 | 0.167 | 0.031 | 3.023 | 0.424 | 0.580 |
| $\Delta_{31}(L)C_-$ | 1.166 | 0.723 | 0.575 | 7.632 | 4.973 | 4.090 |

**Table 1**: Values of $\Delta_{31}(L) \equiv L\Delta m^2_{31}/(4E)$, $C_+$ and $C_-$ for $\Delta m^2_{31} = 3.5 \times 10^{-3}\,\mathrm{eV}^2$, $\sin^2 2\theta_{23} = 1$ and $\sin^2 2\theta_{13} = 0.01$ (see the text).

In general, $\Delta_{31}(L)$ decreases linearly with the increase of $E$. At 1000km matter effects are small. $C_+$ (eq. 14) decreases as $E$ changes from 5 to 15 GeV, approaching the resonance energy from below. Note that due to the matter term we have $C_+ < 1$ and $C_- > 1$ for the three values of $E$ of interest. The argument of the oscillating sine factor in $P^{3\nu}_E(\nu_e \to \nu_\mu)$ and in $P^{3\nu}_E(\bar\nu_e \to \bar\nu_\mu)$ at values of $E$ considered is relatively small allowing an expansion of the sine in the oscillation probability $P^{3\nu}_E(\nu_e \to \nu_\mu) \cong s^2_{23}\sin^2(2\theta_{13})\ (\Delta_{31}(L_0))^2$. The fact that the matter effect factors cancel out reflects the negligibility of matter effects at short baselines[7]. Neglecting matter effects at short baselines, the maximum of the differential event rate spectrum is at one half of the muon beam energy which is 10 GeV in the case under discussion.

At $L = 6000$ km, one has $\Phi(L) = \Phi(L_0)(L_0/L)^2 = \Phi(L_0)/36$, where $\Phi(L)$ is the flux of $\nu_e$ or $\bar\nu_e$ at distance $L \geq L_0$. The argument of the sine is large for the anti-neutrino channel giving for the corresponding rates the upper bound

$$\begin{aligned} dn_{\mu^-}(\mu^+)/dE \propto\ & s^2_{23}\ g_{\bar\nu_e}(x)\ \frac{\Phi(L_0)}{36}\ \frac{\sin^2 2\theta_{13}}{C^2_-}\sin^2\left(\Delta_{31}(L)C_-\right) \\ \leq\ & s^2_{23}\ g_{\bar\nu_e}(x)\ \frac{\Phi(L_0)}{36}\ \frac{\sin^2 2\theta_{13}}{C^2_-}\ . \end{aligned} \tag{30}$$

Obviously, $dn_{\mu^-}(\mu^+)/dE$ is strongly suppressed primarily by the decreasing of the flux. The suppression due to the matter effect term $(1/{C_-}^2)$ for $E = (5-15)\,\mathrm{GeV}$ is by a factor of $\sim (2-5)$. The same conclusion is valid for $dn_{\mu^+}(\mu^-)/dE$ below the resonance region, say at $E = 5$ GeV.

For neutrinos in the resonance region $E \cong (10-15)\,\mathrm{GeV}$, the argument of the sine is small even for very long baselines. Like in the case of short baselines an expansion becomes

[7]Note however that for longer baselines where $\Delta \ll 1$ does no longer hold, the same conclusion would be wrong.

possible:

$$dn_{\mu^+}(\mu^-)/dE \propto \quad s_{23}^2 \; g_{\nu_e}(x) \; \Phi(L_0)(\frac{L_0}{L})^2 \; \frac{\sin^2 2\theta_{13}}{C_+^2} \sin^2(\Delta_{31}(L)C_+)$$

$$\cong \quad s_{23}^2 \; g_{\nu_e}(x) \; \Phi(L_0) \; \sin^2(2\theta_{13}) \; (\frac{\Delta m_{31}^2}{4E} L_0)^2 \; . \tag{31}$$

This is approximately equal to the same differential event rate at short baselines. Thus, in the resonance region ($E \cong (10-15)\,\mathrm{GeV}$) and at sufficiently long baselines ($L \gtrsim 4000$), matter effects lead to a strong suppression of anti-neutrino event rate while keeping the neutrino event rate essentially constant with the change of $L$ from $\sim 1000$km to $\sim 7000$km (see fig. 3). In vacuum, however, the neutrino rate as well as the anti-neutrino rate would show the same strong $(L_0/L)^2$ suppression at long baselines.

For fixed $L \gtrsim 4500$ km, say at $L = 6000$ km, the matter effects lead to a strong enhancement of $dn_{\mu^+}(\mu^-)/dE$ as a function of $E$ in a region which is somewhat wider than the MSW resonance region, $E \sim (8-15)$ GeV, in spite of the fact that in this region $\Delta_{31}(L)C_+ < 0.6$ and

$$dn_{\mu^+}(\mu^-)/dE \propto \quad s_{23}^2 \; g_{\nu_e}(x) \; \Phi(L) \frac{\sin^2 2\theta_{13}}{C_+^2} \sin^2(\Delta_{31}(L)C_+)$$

$$\cong \quad s_{23}^2 \; g_{\nu_e}(x) \; \Phi(L) \; \sin^2 2\theta_{13} \; (\Delta_{31}(L))^2. \tag{32}$$

We have in the indicated energy region $\Delta_{31}(L) > 1$ and the enhancement of $dn_{\mu^+}(\mu^-)/dE$ compared to the case of $\nu_e \leftrightarrow \nu_\mu$ vacuum-oscillations is actually given by the ratio of $(\Delta_{31}(L))^2$ and $\sin^2(\Delta_{31}(L))$.

Fig. 4 shows the results corresponding to fig. 3 for a beam energy of 50 GeV. At very long baselines, the neutrino rate spectrum clearly peaks at the energy where the MSW-resonance condition is fulfilled. The change of the shape of the spectrum with the baseline $L$ is more pronounced now because the resonance energy does not coincide with the maximum of the beam spectrum as it approximately does for a beam energy of 20 GeV. The baseline and muon energy dependence of matter effects will be further discussed in the next section in connection with a quantitative analysis of the significance of the effects shown in figs. 1 and 2.

## 4 Statistical Significance of Matter Effects

We have seen in the previous section that matter effects change the total event rates in the appearance channels $\nu_e \to \nu_\mu$ and $\bar{\nu}_e \to \bar{\nu}_\mu$ in very long baseline experiments in a drastic way. Such experiments would therefore offer unique possibilities to observe matter effects and to test the predictions of the MSW theory. In order to study the capabilities of a neutrino factory experiment quantitatively, we must first define the meaning of "observing matter effects". One of the most interesting possibilities would be a detailed observation of the shape of the neutrino energy spectrum which is modified by the MSW effect in a very characteristic way. This would allow to test non-trivial predictions of the MSW theory and

would allow to unambiguously attribute the enhancement/depletion of the total number of neutrino events to matter effects. High differential event rates and a good calibration of the detector would however be necessary for this option. We will discuss this possibility in sect. 6. In this section we confine ourselves to a discussion of the significance of MSW effects in total event rates.

Matter effects produce deviations of the total number of wrong sign muon events $n_{\mu^+}(\mu^-)$, $n_{\mu^-}(\mu^+)$ from what is expected in the absence of matter. The discussion above clearly shows that such deviations occur in opposite directions in the appearance channels. Suppose that a certain number of wrong sign muon events in the neutrino (antineutrino) appearance channel $n_{\mu^+}(\mu^-)$ ($n_{\mu^-}(\mu^+)$) is measured, while $\langle n^{\rm vac}_{\mu^+}(\mu^-)\rangle$ ($\langle n^{\rm vac}_{\mu^-}(\mu^+)\rangle$) would be expected in the absence of matter effects. We want to determine the confidence level at which $n_{\mu^+}(\mu^-)$ and $n_{\mu^-}(\mu^+)$ could represent statistical fluctuations around the expected values in vacuum $\langle n^{\rm vac}_{\mu^+}(\mu^-)\rangle$, $\langle n^{\rm vac}_{\mu^-}(\mu^+)\rangle$. We follow the procedure proposed by the Particle Data Book [36] and calculate confidence levels by using

$$\begin{aligned}\chi^2 = 2\,\left[\langle n^{\rm vac}_{\mu^+}(\mu^-)\rangle - n_{\mu^+}(\mu^-)\right] + 2n_{\mu^+}(\mu^-)\log\frac{n_{\mu^+}(\mu^-)}{\langle n^{\rm vac}_{\mu^+}(\mu^-)\rangle} \\ +2\,\left[\langle n^{\rm vac}_{\mu^-}(\mu^+)\rangle - n_{\mu^-}(\mu^+)\right] + 2n_{\mu^-}(\mu^+)\log\frac{n_{\mu^-}(\mu^+)}{\langle n^{\rm vac}_{\mu^-}(\mu^+)\rangle} \quad .\end{aligned} \tag{33}$$

The corresponding "number of standard deviations" is given by $n_\sigma \equiv \sqrt{\chi^2}$. This prescription incorporates the available information in both the measured numbers $n_{\mu^+}(\mu^-)$, $n_{\mu^-}(\mu^+)$ in the most complete way. Note that the results which will be shown later with this method in figures 5-7 below assume that $\theta_{13}$ is known with some precision before such an analysis is performed. This could e.g. be realized by a measurement of the $\nu_e \to \nu_\mu$ and/or $\bar\nu_e \to \bar\nu_\mu$ rates at a relatively short baseline, say, below 1000 km. If $\theta_{13}$ were only limited from above then one would have to vary $\theta_{13}$ in the vacuum rates entering the definition of $\chi^2$ in eq. (33) in the allowed range and find the minimum. This would reduce the significance at largest baselines. The statistical method defined above in eq. (33) can be understood intuitively by defining an asymmetry

$$A := \frac{\Delta}{\Sigma} = \frac{n_{\mu^+}(\mu^-) - 2n_{\mu^-}(\mu^+)}{n_{\mu^+}(\mu^-) + 2n_{\mu^-}(\mu^+)} \tag{34}$$

which is obviously very sensitive to effects which affect $n_{\mu^+}(\mu^-)$ and $n_{\mu^-}(\mu^+)$ in a opposite way, while at the same time a number of common systematic effects drop out. For small $\Sigma^{\rm vac}$ (i.e. small beam energies) this method is related to comparing the absolute asymmetry expected in matter with the expected fluctuations of this quantity in the vacuum-case $\chi = \Delta/\delta\Delta^{\rm vac}$. For large $\Sigma^{\rm vac}$ this is equivalent to doing the same with the asymmetry: $\chi = A/\delta A^{\rm vac}$. Note that the sign of $\Delta m^2_{31}$ can be determined from $A$ or equivalently from $\Delta$. This can easily be seen by observing, for example, that for $N_{\mu^+} = N_{\mu^-}$ the difference $P^{3\nu}_E(\nu_e \to \nu_\mu) - P^{3\nu}_E(\bar\nu_e \to \bar\nu_\mu)$, with $P^{3\nu}_E(\nu_e \to \nu_\mu)$ and $P^{3\nu}_E(\bar\nu_e \to \bar\nu_\mu)$ given by eq. (25), enters in $\Delta$. The sign of $\Delta$ and $A$ depends therefore unambiguously on whether $C_+$ or $C_-$ is bigger than one (and the other smaller than one). Via the definition of $C_\pm$ given in eq. (14) this is in turn unambiguously related to the sign of $\Delta m^2_{31}$.

Before we show the numerical results, let us discuss the qualitative dependence of $n_\sigma$ on the relevant parameters. The dependence of $n_\sigma$ on the intensity of the muon source and the detector size and efficiency, as well as the dependence on the mixing parameters follows simply from the previous section:

$$n_\sigma \propto (N_\mu N_{\rm kT} \epsilon_\mu)^{1/2} \quad \text{and} \quad n_\sigma \propto \sin\theta_{23} \sin 2\theta_{13} \ . \tag{35}$$

The dependence of $n_\sigma$ on the baseline $L$ and the muon energy $E_\mu$ is less trivial. In general, matter effects increase with the baseline $L$. Thus a long baseline is essential for the observation of matter effects. For relatively small baselines $L \leq 730\,\text{km}$, in fact, matter effects mostly cancel in eq. (25), thus making such baselines better suited for CP-violation measurements [2, 7]. The dependence on $E_\mu$ needs more explanation and there is also some dependence on the statistical method used. In our simple approach which takes into account only total rates, the significance to matter effects grows first strongly with the increase of the beam energy. At very long baselines, where matter effects are non negligible, a maximum is reached at a beam energy which allows a maximal number of neutrinos to fall into the MSW-resonance energy region. After a small depletion the significance starts to grow again. This is due to the fact that the rates of high energy ($\gtrsim 50\,\text{GeV}$) neutrinos and anti-neutrinos are strongly suppressed due to the matter effects. For large beam energies it is, as was already mentioned earlier, crucial to know the precise value of $\sin^2 2\theta_{13}$. Otherwise it is difficult to distinguish matter suppression from a reduced event rate due to a smaller $\theta_{13}$ in absence of matter effects (see fig. 1 for large L).

The dependence of $n_\sigma$ on $L$ and $E_\mu$ is shown in fig. 5 for $\Delta m^2_{31} = 3.5 \cdot 10^{-3}\,\text{eV}^2$ and $N_\mu N_{\rm kT} \epsilon = 10^{21}$, where the contour lines of $n_\sigma$ are plotted in the $L$-$E_\mu$ plane. The solid

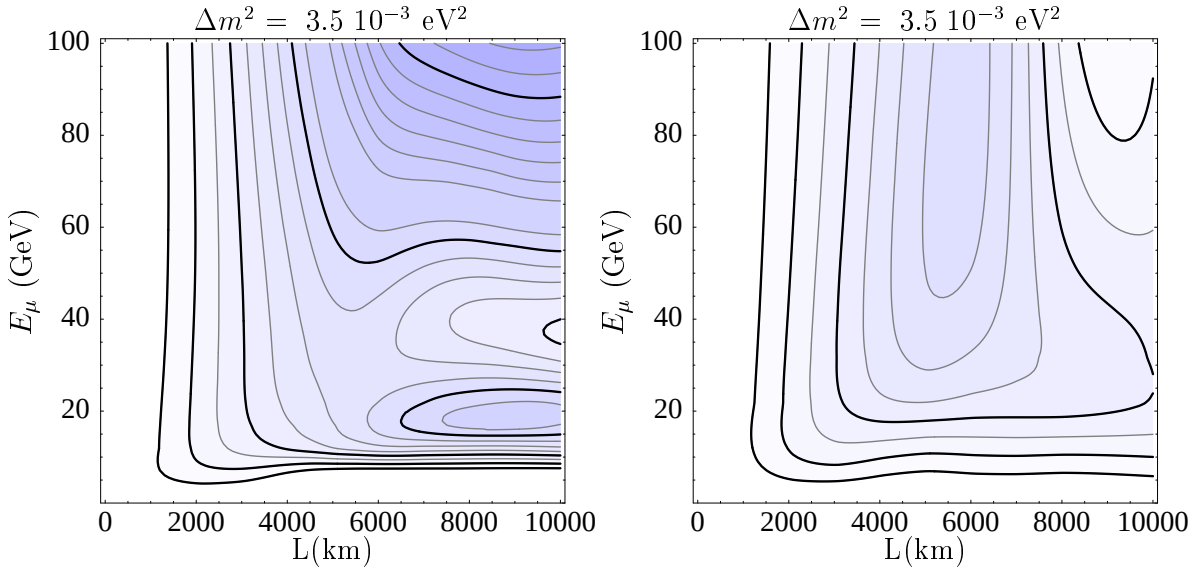


**Figure 5**: *Contour lines of $n_\sigma$ in the $L$-$E_\mu$ plane. We use $\Delta m^2_{31} = 3.5 \cdot 10^{-3}\,\text{eV}^2$ and $N_\mu N_{kT} \epsilon = 10^{21}$ and the solid contour lines correspond to $n_\sigma = 10 \sin 2\theta_{13} \cdot \{1, 2, 4, 8, 16\}$. The left plot assumes that $\theta_{13}$ is known, while the right plot is obtained by varying $\theta_{13}$ in the range currently allowed.*

contour lines correspond to $n_\sigma = 10 \sin 2\theta_{13} \cdot \{1, 2, 4, 8, 16\}$. The left plot assumes that $\theta_{13}$ is known, while the right plot is obtained by varying $\theta_{13}$ in the range currently allowed. With the simple "total rates based" method described above and assuming in the following discussion that $\theta_{13}$ is known, any $L$ from the interval $(4.0 - 10.0) \times 10^3$ km would be suitable for the purpose if $\Delta m^2_{31} = 3.5 \times 10^{-3}\,\mathrm{eV}^2$, $\sin^2 2\theta_{13} = 0.01$ and $E_\mu = 20$ GeV, with the sensitivity to matter effects increasing with $L$. For $E_\mu = 50$ GeV, the sensitivity varies very little for $L \cong (4.0 - 10.0) \times 10^3$ km. Let us note that at $L \gtrsim 3.0 \times 10^3$ km the matter effects are substantial for any neutrino energy $E$ either in the $\nu_e \to \nu_\mu$ and/or in the $\bar{\nu}_e \to \bar{\nu}_\mu$ channel, depending on the sign of $\Delta m^2_{31}$: at $L \gtrsim 3.0 \times 10^3$ km we have $\sqrt{2} G_F \bar{N}^{man}_e L/2 \gtrsim 0.95$. The matter effects can be negligible for certain intervals of neutrino energies for $L \lesssim 2.0 \times 10^3$ km. For relatively large $E$ and $L \lesssim 2.0 \times 10^3$ km, the oscillating factors in $P^{3\nu}_E(\nu_e \to \nu_\mu)$ and $P^{3\nu}_E(\bar{\nu}_e \to \bar{\nu}_\mu)$, eqs. (10), (11), (13) and (14), can be expanded in power series of their arguments and matter effects cancel in the leading orders of these expansions. Moreover, one has $\sin^2(\Delta_{31}(L)) \cong (\Delta_{31}(L))^2$. At $L = 10^3$ km and for $\Delta m^2_{31} = 3.5 \times 10^{-3}\,\mathrm{eV}^2$, $\sin^2 2\theta_{13} = 0.01$, for instance, the earth matter effects cause a difference between $P^{3\nu}_E(\nu_e \to \nu_\mu)$, eq. (10), and the probability of the $\nu_e \to \nu_\mu$ transitions in vacuum $P^{3\nu}_{vac}(\nu_e \to \nu_\mu)$, eq. (5), which does not exceed $\sim 5 \times 10^{-5}$ at $E \geq 10$ GeV. We have, however, $|P^{3\nu}_E(\bar{\nu}_e \to \bar{\nu}_\mu) - P^{3\nu}_{vac}(\bar{\nu}_e \to \bar{\nu}_\mu)| \leq 10^{-4}$ $(10^{-5})$ for $E \geq 10$ (20) GeV. For $\Delta m^2_{31} = 7.0 \times 10^{-3}\,\mathrm{eV}^2$, the same conclusions hold for approximately two times higher neutrino energies. Note that $P^{3\nu}_{vac}(\nu_e \to \nu_\mu) \sim s^2_{23} \sin^2 2\theta_{13}$ and for the values of $\sin^2 2\theta_{13}$ and $s^2_{23}$ used in the above examples we have $s^2_{23} \sin^2 2\theta_{13} = 0.005$. Thus, baselines shorter than about 2000 km and parent muon energies $E_\mu \gtrsim (20 - 25)$ GeV seem to be better suited for searches of CP-violation in neutrino oscillations whose source is the lepton mixing matrix. The magnitude of the asymmetry between the probabilities due to matter effects effectively grows quadratically with the baseline until the argument $\Delta_{31}(L) C_+$ and/or $\Delta_{31}(L) C_-$ approaches and exceeds one [7].

The significance of the effect, i.e. the number of standard deviations $n_\sigma$, depends most crucially on $\theta_{13}$ and $L$. We illustrate this dependence in fig. 6 again for $\Delta m^2_{31} = 3.5 \cdot 10^{-3}\,\mathrm{eV}^2$, where the contour lines corresponding to $n_\sigma = 1, 2, 3, 4, 5$ are plotted in the $\sin^2 2\theta_{13}$-$L$ plane for two values of the product $N_\mu N_{\mathrm{kT}} \epsilon$: $10^{21}$ (left plot) and $10^{22}$ (right plot). The muon energy is in both cases of fig. 6 $E_\mu = 20\,\mathrm{GeV}$, while fig. 7 shows the same plots with identical parameters for $E_\mu = 50\,\mathrm{GeV}$. The vertical dashed lines represent in all these figures the upper limit on $\sin^2 2\theta_{13}$. Figs. 6 and 7 show that matter effects could be observed in the total event rates for given baseline $L$ in a rather large $\sin^2 2\theta_{13}$ interval, while non-observation implies very strong upper bounds on $\sin^2 2\theta_{13}$. Figs. 6 and 7 show in other words the $\sin^2 2\theta_{13}$ range where the enhancement/depletion of the total appearance rates in vacuum due to matter effects is statistically significant for a given confidence level. In those ranges one can not only observe the deviations from the results expected in vacuum, but also the deviation from the results which one would get in matter if the sign of $\Delta m^2_{31}$ were reverted. A measurement of the sign of $\Delta m^2_{31}$ would therefore be possible in the $\sin^2 2\theta_{13}$ range where matter effects are statistically significant at a given confidence level.

Finally we show in figs. 8 and 9 the sensitivity of the statistical significance to the chosen value of $\Delta m^2_{31}$. Fig. 8 is exactly the same plot as fig. 5 with minimal and maximal $\Delta m^2_{31}$. In the left plot we have $\Delta m^2_{31} = 1.0 \cdot 10^{-3}\,\mathrm{eV}^2$ and in the right plot $\Delta m^2_{31} = 8.0 \cdot 10^{-3}\,\mathrm{eV}^2$.

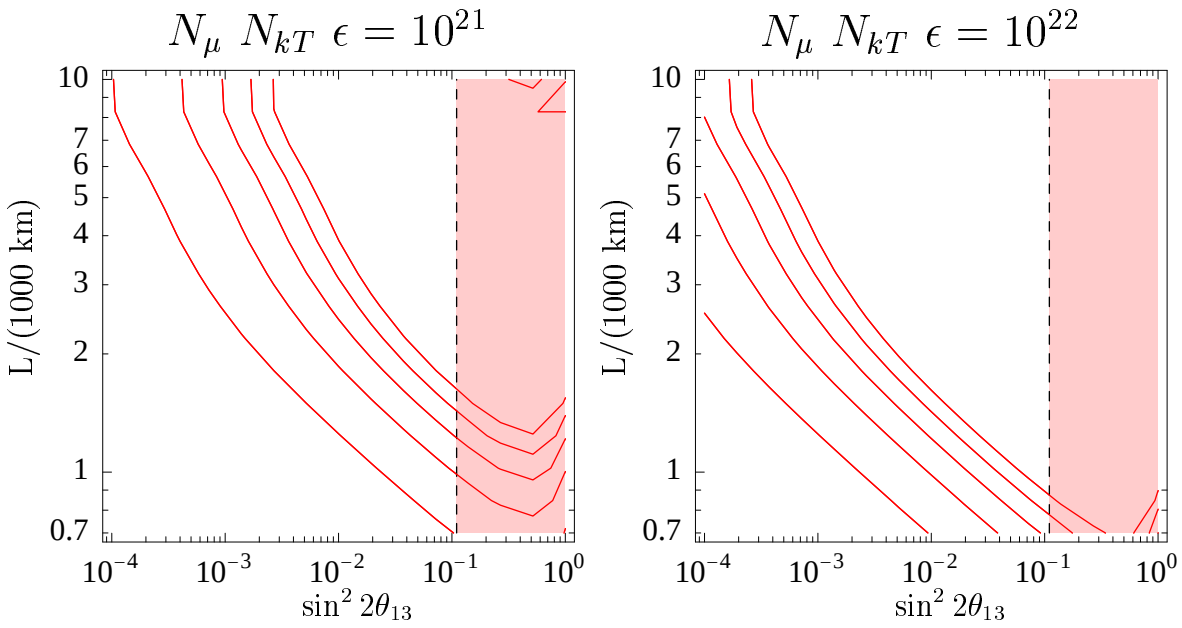


**Figure 6**: *Contour lines of $n_\sigma$ corresponding to $n_\sigma = 1, 2, 3, 4, 5$ in the $\sin^2 2\theta_{13}$-$L$ plane for $E_\mu = 20\,\mathrm{GeV}$ and the two different values $N_\mu N_{kT}\epsilon = 10^{21}$ (left plot) and $N_\mu N_{kT}\epsilon = 10^{22}$ (right plot).*

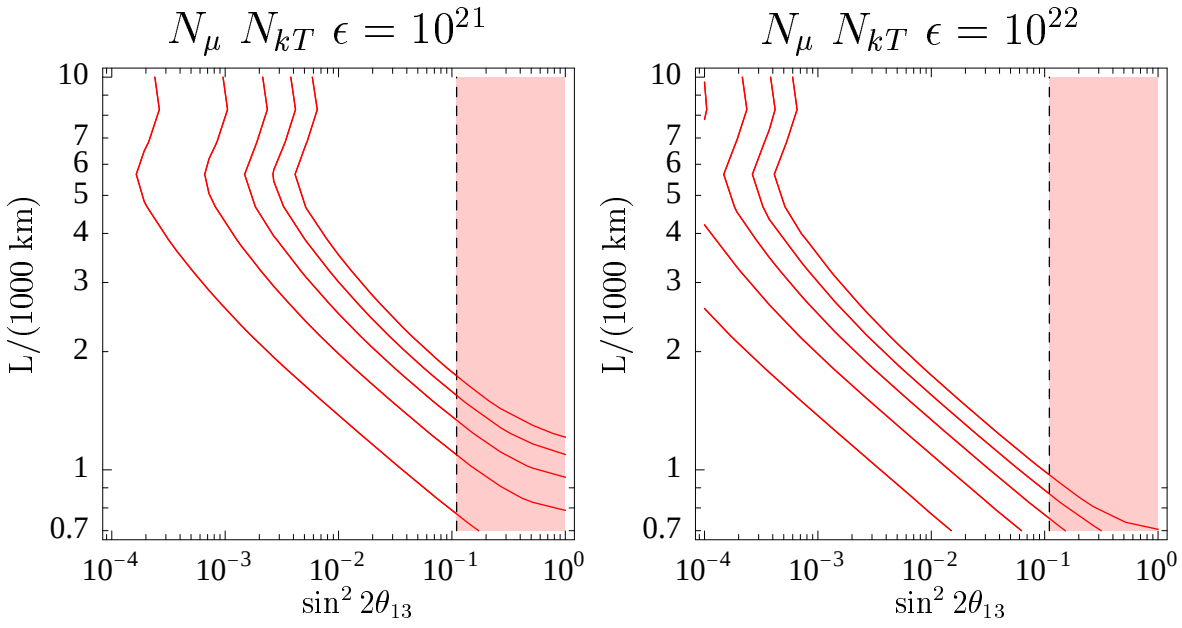


**Figure 7**: *Same as in fig. 6 but for $E_\mu = 50\,\mathrm{GeV}$.*

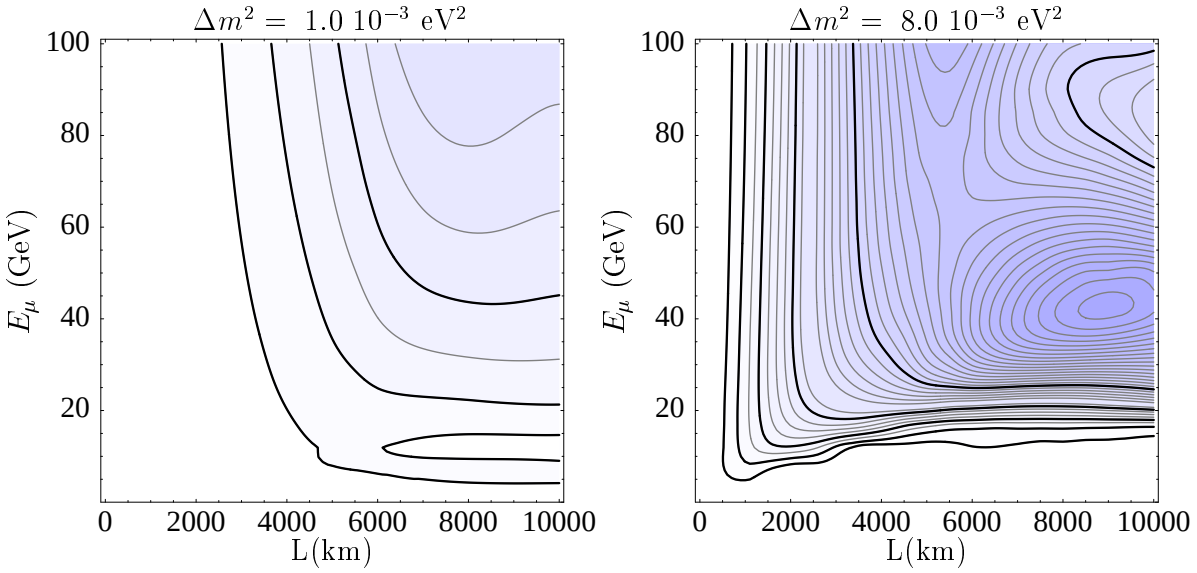


**Figure 8**: *Sensitivity of the statistical significance of matter effects to the value of* $\Delta m^2_{31}$ *analogous to fig. 5. The left plot uses* $\Delta m^2_{31} = 1.0 \cdot 10^{-3}\,\mathrm{eV}^2$ *while for the right plot* $\Delta m^2_{31} = 8.0 \cdot 10^{-3}\,\mathrm{eV}^2$ *with otherwise unchanged parameters. As in fig. 5 the solid contour lines correspond to* $n_\sigma = 10 \sin 2\theta_{13} \cdot \{1, 2, 4, 8, 16\}$.

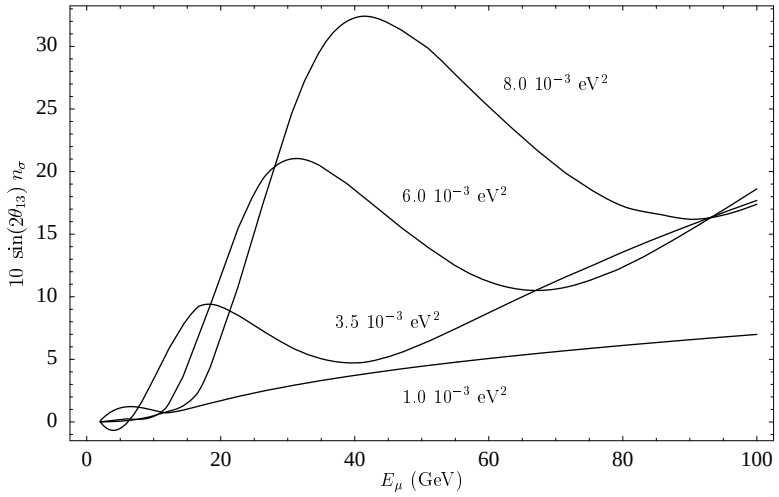


**Figure 9**: *Sensitivity of the statistical significance of matter effects to the value of* $\Delta m^2_{31}$ *for fixed* $L = 8000$ km *as a function of* $E_\mu$. *The lines show* $10 \sin 2\theta_{13} n_\sigma$ *for different* $\Delta m^2_{31}$ *values.*

Fig. 9 shows the statistical significance (i.e. $10 \sin 2\theta_{13} n_\sigma$) for different $\Delta m^2_{31}$ values for $L = 8000$ km as a function of $E_\mu$. For very long baselines, one can see from fig. 9 that increasing $\Delta m^2_{31}$ mainly shifts the resonance energy to higher values thus demanding higher beam energies to reach optimal statistical significance. The local maximum in fig. 8 shifts to 10 GeV for minimal $\Delta m^2_{31}$ and to 40 GeV for maximal $\Delta m^2_{31}$. Improved knowledge of $\Delta m^2_{31}$ would thus in principle allow to discuss optimization issues, but such a study should also include systematics and backgrounds. Moreover, the energy distribution of wrong sign muon events would add important information to the simple counting of events. A detailed discussion of muon energy optimization depends therefore on the way that information will be exploited.

## 5 Subleading $\Delta m^2_{21}$-effects

The results shown so far were obtained in the limit $\Delta m^2_{21} = 0$ which is, as already explained, a perfect approximation for $\Delta m^2_{21} \ll 10^{-4}\,\mathrm{eV}^2$ and/or $\sin^2 2\theta_{12} \ll 1$, i.e. for the VO and SMA MSW solutions of the solar neutrino problem. The LMA MSW solution, that we will consider in this section, allows however $\Delta m^2_{21}$ values up to $2 \cdot 10^{-4}\,\mathrm{eV}^2$ and prefers $\sin^2 2\theta_{12} \simeq 0.8$ [37], so that effects associated to $\Delta m^2_{21}$ can become important, especially for the largest $\Delta m^2_{21}$ values in the LMA range. Two more mixing parameters, namely $\theta_{12}$ and $\delta$, become relevant if $\Delta m^2_{21}$ is non-negligible [32, 38] (see also, e.g., [39]), as the expression for $P^{3\nu}_E(\nu_e \to \nu_\mu)$, eq. (16), including the leading order $\Delta m^2_{21}-$corrections shows. While $\theta_{12}$ is rather constrained, so that we will use $\sin^2 2\theta_{12} = 0.8$ in the following numerical results, any value of $\delta$ in its range $0 \leq \delta < 2\pi$ is allowed at present. As it is clear from eq. (16), in order to calculate the effects associated with a non-negligible $\Delta m^2_{21}$, a value of $\delta$ must be specified. In fig. 10, the total rates in the appearance channels $\nu_e \to \nu_\mu$ (left) and $\bar\nu_e \to \bar\nu_\mu$ (right) for $\Delta m^2_{21} = 0$ (solid line) are compared with the total rates for $\Delta m^2_{21} = 10^{-4}\,\mathrm{eV}^2$ and four possible values of $\delta$ in its range, $\delta = 0,\ \pi/2,\ \pi,\ 3\pi/2$ (dashed lines). As it follows from eq. (16) and these figures, the size of the effects depends crucially on the value of $\theta_{13}$. Fig. 10 assumes a value of $\theta_{13}$ at its upper limit, i.e. $\sin^2 2\theta_{13} = 0.1$, whereas fig. 11 shows the effects for a $\sin^2 2\theta_{13}$ one order of magnitude smaller, $\sin^2 2\theta_{13} = 0.01$. Both figures were obtained for $N_\mu N_{\mathrm{kT}} \epsilon = 10^{21}$.

Figs. 10 and 11 illustrate several interesting features of the $\Delta m^2_{21}$ effects. First of all, a comparison of figs. 10 and 11 confirms that the relative size of the effects grows when $\theta_{13}$ gets smaller [4]. This is because the zeroth order approximations (in $\Delta m^2_{21}$) for the appearance probabilities have a $\sin^2 2\theta_{13}$ suppression, whereas the linear $\Delta m^2_{21}$ corrections (CP-conserving and violating) are suppressed by only one power of $\sin 2\theta_{13}$ (see eqs. (10) and (16)) and the corrections quadratic in $\Delta m^2_{21}$ (CP-conserving) are not suppressed by $\theta_{13}$ at all. Indeed, at sufficiently small $L$ we have $\sin(\Delta \bar E_m L/2) \cong \Delta \bar E_m L/2$, $\sin(\bar\kappa + \Delta \bar E_m L/2) \cong (\bar\kappa + \Delta \bar E_m L/2)$, etc., and as can be shown [34], the leading CP-conserving and CP-violating $\Delta m^2_{21}-$corrections containing the factor $\cos\theta'_{12}$ in eq. (16) reduce essentially to their vacuum oscillation form:

$$\Delta P^{3\nu}_E(\nu_e \to \nu_\mu;\ \delta) \cong \quad 8 J^V_{CP} \left(\frac{L}{2}\frac{\Delta m^2_{21}}{2E}\right) \left(\frac{L}{2}\frac{\Delta m^2_{31}}{2E}\right) \quad \left[\cot\delta \ - \ \frac{L}{2}\frac{\Delta m^2_{31}}{2E}\right] \qquad (36)$$

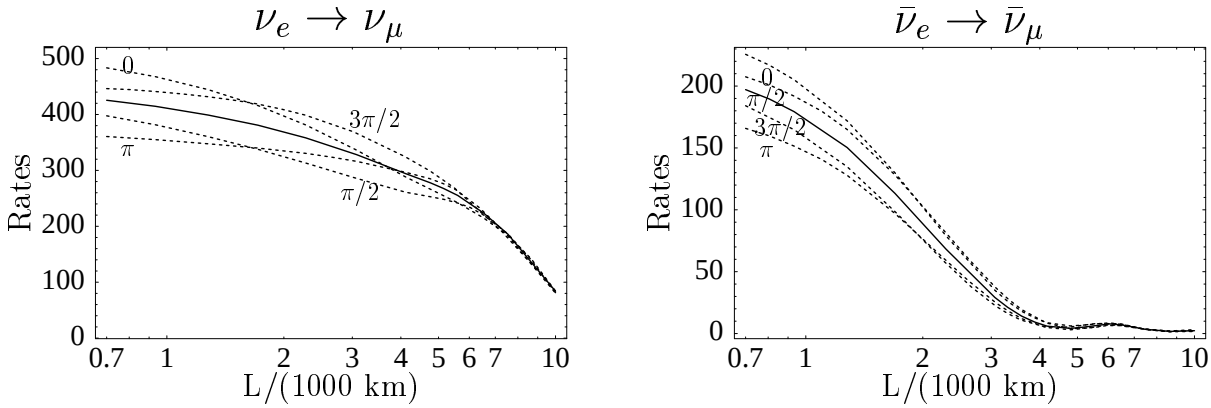


**Figure 10**: *Appearance event rates $n_{\mu^+}(\mu^-)$, $n_{\mu^-}(\mu^+)$ in matter with subleading $\Delta m^2_{21} = 10^{-4}\,\mathrm{eV}^2$ and four possible values of the CP-phase $\delta = 0,\ \pi/2,\ \pi,\ 3\pi/2$ against baseline $L$ (dashed lines) compared with the corresponding event rates with negligible $\Delta m^2_{21}$ (solid lines) for the channels $\nu_e \to \nu_\mu$ (left) and $\bar{\nu}_e \to \bar{\nu}_\mu$ (right). Both figures correspond to $N_\mu = 2{\cdot}10^{20}$, $\epsilon = 50\%$, $E_\mu = 20\,\mathrm{GeV}$, $\sin^2 2\theta_{23} = 1$, $\sin^2 2\theta_{12} = 0.8$ and $\sin^2 2\theta_{13} = 0.1$.*

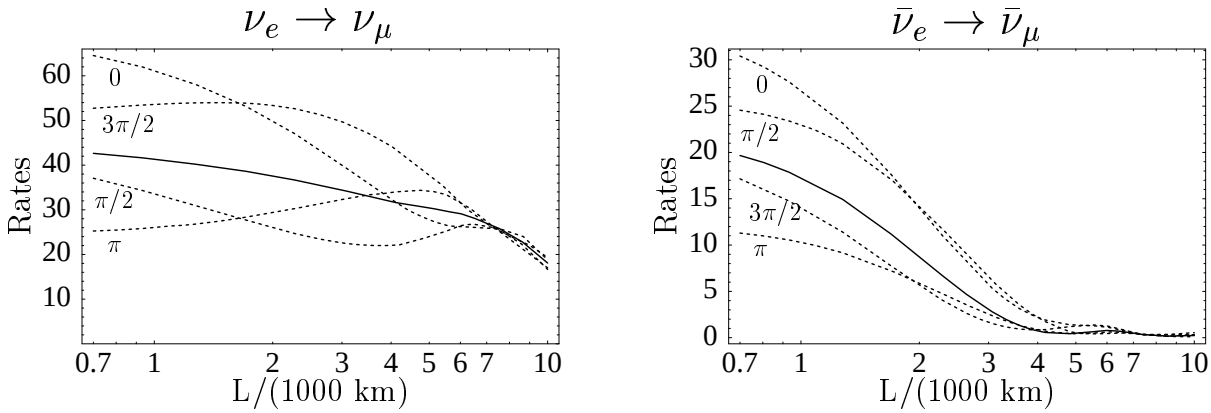


**Figure 11**: *Same as fig. 10 but for* $\sin^2 2\theta_{13} = 0.01$.

where

$$J^V_{CP} = \frac{1}{8}\sin\delta\ c_{13}\sin 2\theta_{12}\sin 2\theta_{13}\sin 2\theta_{23} \tag{37}$$

is the CP-violation rephasing invariant of the lepton mixing matrix [32].

Unlike the appearance channels, the disappearance channels are dominated by the transitions to $\nu_\tau$ ($\bar{\nu}_\tau$) and are therefore not suppressed by $\theta_{13}$ or $\Delta m^2_{21}$, so that the $\theta_{13}$-suppressed $\Delta m^2_{21}$ corrections are much less significant in this case. Figs. 10 and 11 show also that the range of the $\Delta m^2_{21}$ corrections is essentially determined by $\theta_{13}$, but the precise size and sign of these corrections within this range is unknown if $\delta$ is unconstraint. This can be seen also explicitely in figs. 10 and 11 where the $\Delta m^2_{21}$ corrections show up as oscillations around

the leading $\Delta m^2_{31}$ contribution to the rates (dashed line), whose initial phase depends on $\delta$. The $\Delta m^2_{21}$ effects represent consequently in the present LMA scenario in a high statistics long-but-not-too-long baseline measurement of $\theta_{13}$ an important source of systematic error, unless $\delta$ is measured [4, 7]. On the other hand, $\sin\delta$ could be measured or constrained in this scenario by comparing the rates in the two CP-conjugated channels $\nu_e \to \nu_\mu$ and $\bar{\nu}_e \to \bar{\nu}_\mu$ if very high intensity sources and large detectors will become available [7]. By comparing e.g. the left and right plots of in fig. 11 one can see that, as it follows from eq. (16), the $\Delta m^2_{21}$ correction has the same sign in the two channels for the two CP-conserving values $\delta = 0,\ \pi$, when $\sin\delta = 0$, but has opposite sign for the two CP-violating values $\delta = \pi/2,\ 3\pi/2$, i.e. when $\sin\delta = \pm 1$.

Note, however, that a measurement of $\delta$ based on a comparison of CP-conjugated rates at a single value of $L$ could not be enough in order to keep the $\Delta m^2_{21}$ effects under control. Suppose, for example, that $\delta = 0$ or $\delta = \pi$. Then the $\Delta m^2_{21}$ effects would be the same in the two channels and an ideal experiment looking for CP-violation would measure $\sin\delta = 0$. The value of $\delta$ would, however, still be undetermined for the simple reason that both $\delta = 0$ and $\delta = \pi$ give $\sin\delta = 0$. As a consequence, it would be still unknown whether the $\Delta m^2_{21}$ corrections in both channels add ($\delta = 0$) or subtract ($\delta = \pi$) to the leading $\Delta m^2_{31}$ contribution to the rates and this ambiguity would translate, e.g., in an uncertainty on a measurement of $\theta_{13}$. Such an ambiguity could be resolved by comparing rates measured at different distances $L$. Fig. 11 for $\sin^2 2\theta_{13} = 0.01$ shows in the $\nu_e \to \nu_\mu$ channel that the change in rates between $L = 3000\,\mathrm{km}$ and $L = 700\,\mathrm{km}$ allows to discriminate between $\delta = 0$ and $\delta = \pi$. Fig. 10 shows that the different $L$ dependence is also significant for $\sin^2 2\theta_{13} = 0.1$, allowing also to distinguish between the two possibilities $\delta = 0$ and $\delta = \pi$. If CP-violation were maximal, $|\sin\delta| = 1$, the comparison of the rates at different baselines would be less significant but still helpful. Figs. 10 and 11 show finally also that the $\Delta m^2_{21}$ effects become smaller when $L$ is increased.

## 6 Matter Effects in the Energy Spectrum.

Motivated by the small differential event rates, we discussed so far only the influence of matter effects on the total rates of wrong sign muon events. We demonstrated in the previous chapters that statistical significant deviations from the total event rates in vacuum represent already a good test of the MSW theory. A significant test would however be also given by a detailed measurement of MSW effects in the neutrino energy spectrum, which is modified in a very characteristic way. The $\nu_\mu \to \nu_\mu$ and $\bar{\nu}_\mu \to \bar{\nu}_\mu$ disappearance channels are again dominated by transitions to $\nu_\tau$ and $\bar{\nu}_\tau$ while $\nu_e$ and $\bar{\nu}_e$ transitions are only small corrections. These channels are therefore mostly insensitive to matter effects in the differential event rate spectrum and will not be discussed further.

To understand the effects in the appearance spectrum of $\nu_e \to \nu_\mu$ and $\bar{\nu}_e \to \bar{\nu}_\mu$ we us again the approximation $\Delta m^2_{21} = 0$. Matter effects have no influence on the angle $\theta_{23}$ in this case, whereas they modify the mixing due to $\theta_{13}$ significantly. One obtains thus for the $\nu_e \to \nu_\mu$ and $\bar{\nu}_e \to \bar{\nu}_\mu$ appearance channels the usual two flavour picture where $\sin 2\theta_{13} \to \sin 2\theta^{\mathrm{m}}_{13} = \sin 2\theta_{13}/C_\pm$, and where $C_+$ corresponds to neutrinos, $C_-$ to antineutrinos. The enhancement

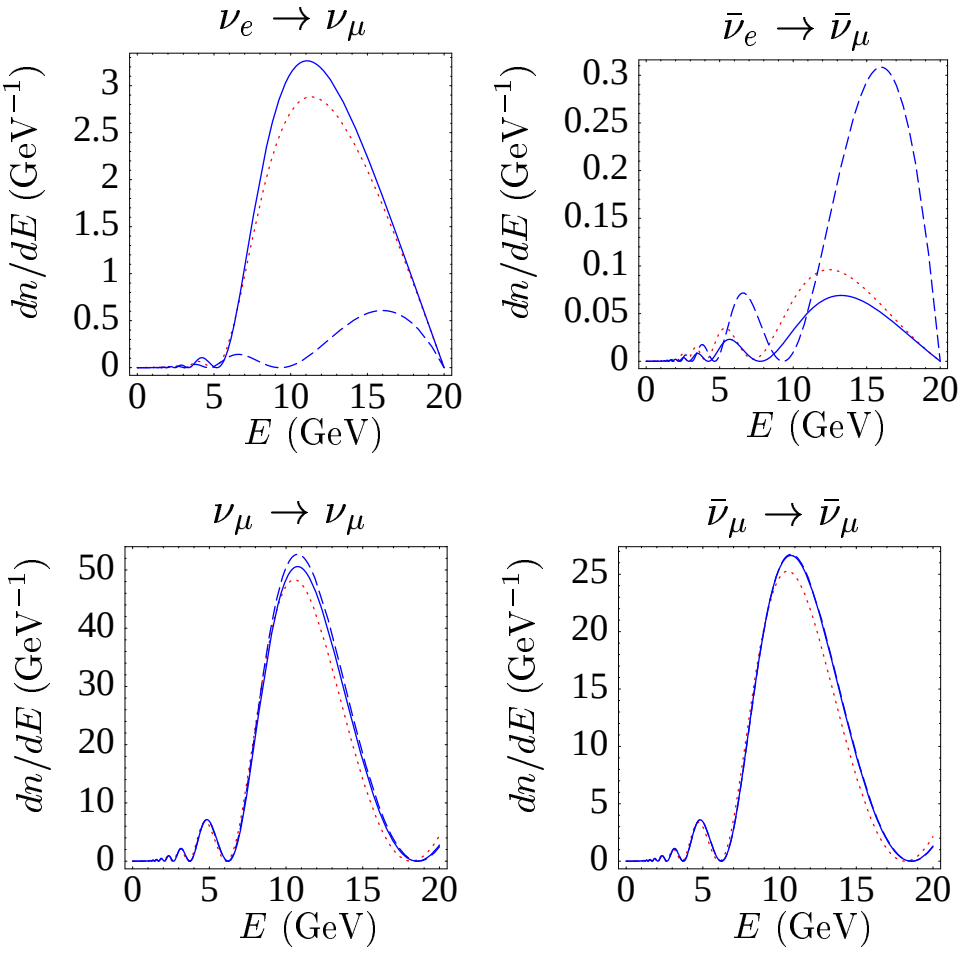


**Figure 12**: *Modifications in the differential event rate spectrum (events per* GeV*) due to matter effects for* $E_\mu = 20\,\mathrm{GeV}$*. The solid lines correspond to oscillations taking place in the earth mantle, while the dashed lines are for oscillations in vacuum, with* $\Delta m^2_{21} = 0$ *in both cases. The "enhancement", the "broadening" and the "shift" of the first oscillation maximum in the* $\nu_e \to \nu_\mu$ *channel as* $E$ *decreases, caused by the MSW effect, is clearly seen. The dotted lines show for comparison an example of* $\Delta m^2_{21}$ *corrections for* $\Delta m^2_{21} = 10^{-4}$ eV$^2$*,* $\delta = 0$ *and* $\sin^2 2\theta_{12} = 0.8$*. The assumed parameters are in all cases* $N_\mu N_{kT} \epsilon = 10^{21}$*,* $L = 6596\,km$ *(CERN-MINOS),* $\Delta m^2_{31} = 3.5x10^{-3}$ eV$^2$ *and* $\sin^2 2\theta_{13} = 0.01$*.*

of $\theta^m_{13}$ is maximal in the neutrino channel when the neutrino energy $E$ coincides with the MSW resonance energy $E_{\rm res}$ defined via:

$$\frac{2E_{\rm res}V}{\Delta m^2_{31}} = \cos 2\theta_{13}\ . \tag{38}$$

Note however that the maximum of the event spectrum in the $\nu_e \to \nu_\mu$ channel does in general not coincide with $E_{\rm res}$ since the MSW oscillation probabilities are folded with the fluxes and cross sections. The maximum of the event spectrum is thus determined by the

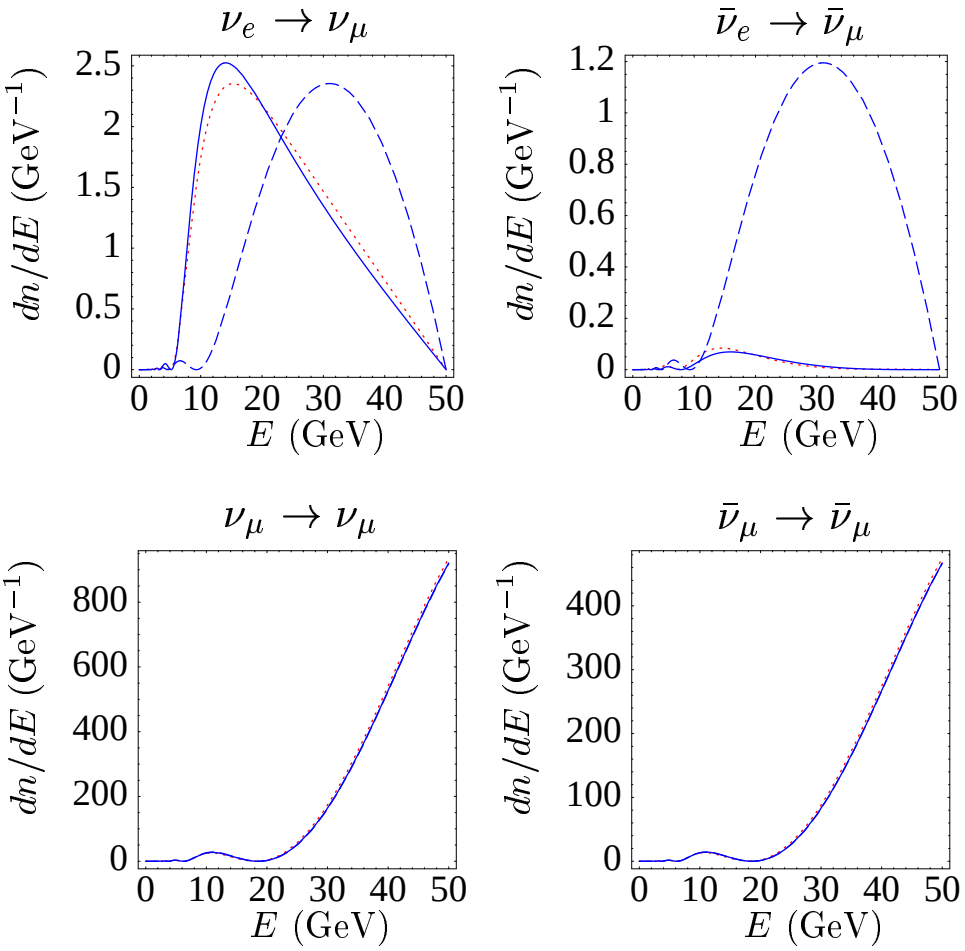


**Figure 13**: *Same as in fig. 12 but for* $E_\mu = 50\,\mathrm{GeV}$. *For details see text.*

maximization of

$$\left(\frac{\sin(\Delta_{31} C_\pm)}{C_\pm}\right)^2 f_{\nu_e\nu_\mu}(E/E_\mu)\ , \tag{39}$$

but the resulting maximum is for the muon energies under consideration still around $E_{\mathrm{res}}$. The offset depends in a rough approximation on the difference between $E_{\mathrm{res}}$ and the maximum of the flux which lies roughly at an energy of the order $E_\mu$.

This has to be compared with the vacuum case where the oscillation probabilities are also folded with fluxes and cross sections and where the maxima of the event rates are also not precisely at the maxima of the oscillation probabilities. The event rate spectrum is thus due to this folding in both cases with and without matter a rather complicated function of $E_\nu$ which depends in a non-trivial way on $L$, $E_\mu$ and $\Delta m^2_{31}$. Nevertheless for given $L$, $E_\mu$ and for given $\Delta m^2_{31}$, $\theta_{23}$, $\theta_{13}$ measured with a suitable long baseline experiment, one can predict the shape of the differential event rate spectrum in all channels and compare it with the spectrum of oscillations unaffected by matter. This results in a very good opportunity

to detect specific details of the MSW effect which arise when the oscillation parameters are chosen such that the first maximum of vacuum oscillation coincides roughly with $E_{\rm res}$. The point is that the MSW effect changes the probabilities compared to vacuum in three genuine ways: The first maximum of the oscillation probability as the energy decreases is enhanced, its width is broadened and its center is shifted to lower energies. Similarly one has an "anti–MSW effect" in the antineutrino appearance channel which implies for the first oscillation maximum a reduction in height, again a broadening and a shift to lower energies.

These "genuine MSW effects" are demonstrated in fig. 12 (where $E_\mu = 20\,\text{GeV}$) and fig. 13 (with $E_\mu = 50\,\text{GeV}$) showing the modifications in the energy spectrum (events per GeV) due to matter effects. The solid lines are in matter while the dashed lines are without matter and the assumed parameters are $N_\mu N_{\rm kT}\epsilon = 10^{21}$ as before, $L = 6596\,\text{km}$ and $\sin^2 2\theta_{13} = 0.01$. Fig. 12 shows already all effects due to the MSW mechanism, namely the broadening (the last oscillation in matter covers two oscillations in vacuum), the shift (the maximum in matter lies almost in the minimum in vacuum) and the enhancement or suppression compared to vacuum. Figs. 12 and 13 also include an example of $\Delta m^2_{21}$ corrections to the spectrum in the LMA scenario (dotted lines). Size and sign of the corrections depend on the value of the phase $\delta$. The dotted line assumes $\delta = 0$ and moreover $\Delta m^2_{21} = 10^{-4}\,\text{eV}^2$ and $\sin^2 2\theta_{12} = 0.8$. As already observed in the previous section, the $\Delta m^2_{21}$ corrections are relatively small for the very long baselines considered here.

It is interesting to look at the modifications when the muon energy becomes higher, e.g. for $E_\mu = 50\,\text{GeV}$ as shown in fig. 13. The point is that the beam energy is already rather far away from the MSW resonance energy and the importance of the weight function $f_{\nu_e\nu_\mu}$ (and of the $E^3_\nu$ scaling of unoscillated events) in the determination of the shape of the spectrum increases. Thus the genuine broadening, shift and enhancement/suppression effects become harder to distinguish. For the $\nu_e \to \nu_\mu$ channel the effect could be hard to distinguish from uncertainties (with low statistics) in the spectrum. This brings up the general issue that one has to have enough statistics for such an analysis. In order to have a chance to see such effects one has to be lucky and $\theta_{13}$ should be at the upper experimental limit (see scaling laws). Otherwise $N_\mu N_{\rm kT}\epsilon$ must be increased correspondingly which implies a more intense muon source, a larger detector or both. Although a more quantitative analysis of the significance of effects in the differential neutrino event rate spectrum is beyond the scope of this paper, an analysis of the differential event rate spectrum would clearly provide extremely valuable additional information which would allow to test some of the characteristic features of the MSW mechanism.

## 7 Conclusions

Assuming three-neutrino mixing we studied in this paper the possibility to test the MSW effect in terrestrial very long baseline neutrino oscillation experiments which become possible with neutrino factories. Such direct tests are important since the MSW mechanism is widely used in different scenarios of neutrino physics and astrophysics. The correct analysis and interpretation of the data from terrestrial very long baseline neutrino oscillation experiments, $L \gtrsim 1000$ km, is in fact impossible without a proper treatment of matter effects. The latter is

also crucial for the searches of CP-violation in neutrino oscillations generated by the lepton mixing matrix, since matter effects create an asymmetry between the two CP-conjugated appearance channels.

Studies of the $\nu_e \to \nu_\mu$ and $\bar{\nu}_e \to \bar{\nu}_\mu$ oscillations are by far most promising for the detection of the matter effects since the corresponding total event rates are affected in a drastic way by these effects. We considered for the present study neutrino trajectories through the earth which cross the mantle, but do not pass through the earth core, which corresponds to neutrino path lengths $L \lesssim 10600$ km. Using analytic expressions for the three neutrino oscillation probabilities in matter in the constant average density and small $\Delta m^2_{21}$ approximations and including fluxes, cross sections and detection efficiencies allows to describe the relevant event rates analytically. This permitted a full analytic understanding of our numerical results.

By considering the asymmetry between the $\nu_e \to \nu_\mu$ and $\bar{\nu}_e \to \bar{\nu}_\mu$ induced wrong sign muon event rates, we studied the statistical significance of the observation of matter effects as a function of the neutrino oscillation parameters $\theta_{13}$ and $\Delta m^2_{31}$ as well as its dependence on the experimental conditions via the parent muon beam energy $E_\mu$, the path length $L$ and the product of useful muons, detector size and efficiency. The scaling of rates, statistical significances and sensitivities with the relevant mixing angles, in particular, with $\theta_{13}$, the intensity of the muon source and with the detector size and efficiency have been given, so that the results for any value of those parameters can easily be obtained. The sign of the asymmetry depends on whether the two closest neutrino mass eigenstates are lighter ($\Delta m^2_{31} > 0$) or heavier ($\Delta m^2_{31} < 0$) than the third one, thus providing a way of determining which of these two possibilities is realized. Figs. 6 and 7 show the conservative ranges of $\sin^2 2\theta_{13}$ where that determination would be significant at a given confidence level from the statistical point of view as function of the baseline.

We analyzed, in particular, the statistical significance of matter effects as a function of $E_\mu$ and $L$. The most important requirement regarding the muon energy is that for given $\Delta m^2_{31}$ it has to be greater than the MSW resonance energy. For, e.g., $\Delta m^2_{31} \leq 6.0\ (8.0) \times 10^{-3}\ \mathrm{eV}^2$, this implies $E_\mu \gtrsim 20\ (30)$ GeV. Using a simple "total rates based" method and assuming that $\theta_{13}$ is known, any $L$ from the interval $(4.0 - 10.0) \times 10^3$ km gives relatively good sensitivity to matter effects if $\Delta m^2_{31} = 3.5 \times 10^{-3}\,\mathrm{eV}^2$, $\sin^2 2\theta_{13} = 0.01$ and $E_\mu = 20$ GeV, with the sensitivity increasing with $L$. For $E_\mu = 50$ GeV, the sensitivity varies very little for $L \cong (4.0 - 10.0) \times 10^3$ km. Let us note that if $\Delta m^2_{31} \simeq 10^{-3}$ eV$^2$ and $\sin^2 2\theta_{13} \lesssim 0.01$, then establishing the matter effects (or obtaining a stringent upper limit on $\sin^2 2\theta_{13}$) would require $E_\mu \simeq (40 - 50)$ GeV. As our results show, the optimal value of $E_\mu$ depends on the precise value of $\Delta m^2_{31}$.

Our analysis shows that a higher sensitivity to the MSW effect in the case of relatively small values of $\sin^2 2\theta_{13}$ is achieved at very large $L$. We showed that this conclusion holds also when subleading $\Delta m^2_{21}$ effects are included. These effects can be significant in the case of the LMA MSW solution with $\Delta m^2_{21} \simeq (0.5 - 2.0) \times 10^{-4}$ eV$^2$. At very large $L$, the indicated $\Delta m^2_{21}$-induced effects are essentially negligible and the results obtained in the limit of $\Delta m^2_{21} = 0$ are therefore sufficiently accurate. This is valid even in the case of the LMA MSW solution with $\Delta m^2_{21} \simeq (0.5 - 2.0) \times 10^{-4}$ eV$^2$. For shorter baselines, $\Delta m^2_{21}$ effects are non-negligible and a determination of the CP-violating phase $\delta$ would be

necessary in order to know their precise magnitude. We have found that the $L$ dependence of the $\Delta m^2_{21}$ effects offers the possibility to determine the CP-phase $\delta$, especially when $\sin\delta$ is small. For $\sin^2 2\theta_{13} = 0.01$, for instance, the event rates due to the $\nu_e \to \nu_\mu$ and $\bar{\nu}_e \to \bar{\nu}_\mu$ transitions change considerably when $L$ changes from $\sim 700$ km to $\sim 3000$ km. Thus, a measurement of these rates, e.g., at the indicated two distances could allow to determine the value of $\delta$ with a certain precision. Finally we discussed the matter effects in the differential event rate spectrum as a function of the neutrino energy, and showed that they lead to very characteristic distortions. The observation of these distortions would allow very detailed tests of the MSW theory.

To conclude, our study shows that the predictions of the MSW theory can be tested in a statistically reliable way in a large region of the corresponding parameter space by a simple analysis of the total event rates in a very long baseline neutrino oscillation experiment. This can allow to determine the sign of $\Delta m^2_{31}$ as well, as was recently noticed also in [8]. Not seeing the matter effects would lead to impressive upper limits on the mixing angle $\theta_{13}$ down to $\sin^2 2\theta_{13} \simeq 10^{-4}$ or even better.

Acknowledgments: A.R. and S.P. wish to thank the Institute T30d at the Physics Department of the Technical University of Munich for warm hospitality.

## References


[1] S. Geer, Phys. Rev. **D57** (1998) 6989, (E) *ibid.* **D59** (1999) 039903.

[2] A. De Rujula, M.B. Gavela and P. Hernandez, Nucl. Phys. **B547** (1999) 21.

[3] V. Barger, S. Geer and K. Whisnant, e-Print Archive: hep-ph/9906487.

[4] K. Dick, M. Freund, M. Lindner and A. Romanino, Nucl. Phys. **B562** (1999) 29.

[5] M. Campanelli, A. Bueno and A. Rubbia, e-Print Archive: hep-ph/9905240.

[6] A. Donini, M.B. Gavela, P. Hernandez and S. Rigolin, e-Print Archive: hep-ph/9909254.

[7] A. Romanino, e-Print Archive: hep-ph/9909425, to be published in Nucl. Phys **B**.

[8] V. Barger, S. Geer, R. Raja and K. Whisnant, e-Print Archive: hep-ph/9911524.

[9] Nufact '99 Workshop, July 5–9th, Lyon. See e.g. the Summary of Detector/Neutrino Beam Parameters by D. Harris, http://lyopsr.in2p3.fr/nufact99/talks/harrisconc.ps.gz.

[10] P. Lipari, e-Print Archive: hep-ph/9903481.

[11] M. Narayan and S.U. Sankar, Phys. Rev. **D61** (2000) 013003.

[12] F.D. Stacey, *Physics of the Earth*, $2^{nd}$ edition, John Wiley and Sons, New York, 1977.

[13] A.D. Dziewonski and D.L. Anderson, Phys. Earth Planet. Interiors **25** (1981) 297.

[14] S.T. Petcov, Phys. Lett. **B434** (1998) 321, (E) *ibid.* **B444** (1998) 584.

[15] M. Maris and S.T. Petcov, unpublished.

[16] M. Freund and T. Ohlsson, e-Print Archive: hep-ph/9909501.

[17] I. Mocioiu and R. Shrock, e-Print Archive: hep-ph/9910554.

[18] A.K. Mann and H. Primakoff, Phys. Rev. **D15** (1977) 655;
V.K. Ermilova, V.A. Tsarev V.A. Chechin, Zh.Eksp.Teor.Fiz. (Pis'ma) **43** (1986) 3531;
P.I. Kratsev, Il Nuovo Cimento **103 A** (1990) 361.

[19] See e.g. "Detectors working group + Neutrinos Beam Parameters Working Group" in the proceeding of the Nufact '99 Workshop, July 5–9th, Lyon, or the "Oscillation Detectors" working group web page at http://www.cern.ch/muonstoragerings/.

[20] G.L. Fogli, E. Lisi, D. Montanino and A. Palazzo, e-Print Archive: hep-ph/9912231 and 9910387; M. Nakahata, in *TAUP'99*, VIth Internationa Workshop on Topics in Astroparticle and Underground Physics, September 6 - 10, 1999, Paris, France, to appear (transparanceis available at http://taup99.in2p3.fr/TAUP99/).

[21] K. Scholberg, for the Super-Kamiokande Collab., e-Print Archive: hep-ex/9905016.

[22] A. De Rujula, M. Lusignoli, L. Maiani, S.T. Petcov and R. Petronzio, Nucl. Phys. **B168** (1980) 54.

[23] S.M. Bilenky and S.T. Petcov, Rev. Mod. Phys. **59** (1987) 671.

[24] M. Apollonio et al. (CHOOZ collaboration), e-Print Archive: hep-ex/9907037.

[25] C.-S. Lim, Report BNL 52079 (1987).

[26] S.T. Petcov, Phys. Lett. **B214**, (1988) 259.

[27] T.K. Kuo and J. Pantaleone, Phys. Rev. Lett. **57** (1986) 1805;
S.T. Petcov and S. Toshev, Phys. Lett. **B187** (1987) 120;
A. Yu. Smirnov, Yad. Fiz. **46** (1987) 1152;
see also: S. Toshev, Phys. Lett. **B185** (1987) 177, (E) *ibid.* B**192** (1987) 478;
C.W. Kim, S. Nussinov and W.K. Sze, Phys. Lett. **B184** (1987) 403;
A. Baldini and G.F. Giudice, Phys. Lett. **B186** (1987) 211.

[28] S.T. Petcov, Invited talk given at the Int. Workshop on Weak Interaction and Neutrinos, January 25 - 30, 1999, Cape Town, South Africa (to be published in the Proceedings of the Workshop), e-Print Archive: hep-ph/9907216.

[29] O. Yasuda, e-Print Archive: hep-ph/9910428.

[30] S.M. Bilenky, J. Hosek and S.T. Petcov, Phys. Lett. **B94** (1980) 495;
P. Langacker, S.T. Petcov, G. Steigman and S. Toshev, Nucl. Phys. B**282** (1987) 589.

[31] M. V. Chizhov, M. Maris and S. T. Petcov, e-Print Archive: hep-ph/9810501.

[32] P.I. Krastev and S.T. Petcov, Phys. Lett. **B205** (1988) 84.

[33] E.K. Akhmedov, A. Dighe, P. Lipari and A.Yu. Smirnov, Nucl. Phys. **B542** (1999) 3.

[34] S.T. Petcov, in preparation.

[35] A. Cervera Villanueva, F. Dydak and J. Gómez-Cadenas, Nufact '99 Workshop, July 5–9th, Lyon, http://lyopsr.in2p3.fr/nufact99/talks/cervera.ps.gz.

[36] C. Caso et al., The European Physical Journal **C3** (1998) 1, and 1999 off-year partial update for the 2000 edition available on the Particle Data Group WWW pages (URL: http://pdg.lbl.gov/).

[37] M.C. Gonzalez-Garcia, P.C. de Holanda, C. Pena-Garay and J.W.F. Valle, e-Print Archive: hep-ph/9906469.

[38] P.K. Kuo and J. Pantaleone, Phys. Lett. **B198** (1987) 406.

[39] M. Koike and J. Sato, e-Print Archive: hep-ph/9909469 and hep-ph/9911258.